

A myeloid tumor suppressor role for *NOL3*

Robert F. Stanley,^{1*} Richard T. Piszczatowski,^{1*} Boris Bartholdy,¹ Kelly Mitchell,¹ Wendy M. McKimpson,¹ Swathi Narayanagari,¹ Dagmar Walter,¹ Tihomira I. Todorova,¹ Cassandra Hirsch,^{7,8} Hideki Makishima,^{7,8} Britta Will,^{1,4,5,6} Christine McMahon,² Kira Gritsman,^{1,4,5,6} Jaroslaw P. Maciejewski,^{7,8} Richard N. Kitsis,^{1,3,4,5,6} and Ulrich Steidl^{1,4,5,6}

¹Department of Cell Biology, ²Department of Pathology, ³Wilf Family Cardiovascular Research Institute, ⁴Albert Einstein Cancer Center, and ⁵Institute for Stem Cell and Regenerative Medicine Research, Albert Einstein College of Medicine, Bronx, NY 10461

⁶Department of Medicine, Albert Einstein College of Medicine–Montefiore Medical Center, Bronx, NY 10461

⁷Department of Translational Hematology and Oncology Research and ⁸Leukemia Program, Cleveland Clinic, Taussig Cancer Institute, Cleveland, OH 44195

Despite the identification of several oncogenic driver mutations leading to constitutive JAK–STAT activation, the cellular and molecular biology of myeloproliferative neoplasms (MPN) remains incompletely understood. Recent discoveries have identified underlying disease-modifying molecular aberrations contributing to disease initiation and progression. Here, we report that deletion of *Nol3* (*Nucleolar protein 3*) in mice leads to an MPN resembling primary myelofibrosis (PMF). *Nol3*^{−/−} MPN mice harbor an expanded Thy1⁺LSK stem cell population exhibiting increased cell cycling and a myelomonocytic differentiation bias. Molecularly, this phenotype is mediated by *Nol3*^{−/−}-induced JAK–STAT activation and downstream activation of *cyclin-dependent kinase 6* (*Cdk6*) and *Myc*. *Nol3*^{−/−} MPN Thy1⁺LSK cells share significant molecular similarities with primary CD34⁺ cells from PMF patients. *NOL3* levels are decreased in CD34⁺ cells from PMF patients, and the *NOL3* locus is deleted in a subset of patients with myeloid malignancies. Our results reveal a novel genetic PMF-like mouse model and identify a tumor suppressor role for *NOL3* in the pathogenesis of myeloid malignancies.

INTRODUCTION

Myeloproliferative neoplasms (MPNs) are a group of related but heterogeneous clonal hematopoietic malignancies that can be classified by the presence of the Philadelphia chromosome (Ph). Ph[−] MPNs include essential thrombocythemia (ET), polycythemia vera (PV), and primary myelofibrosis (PMF). ET and PV are characterized by increased platelet counts and erythrocyte counts, respectively, whereas PMF is characterized by peripheral cytopenias, extramedullary hematopoiesis, and bone marrow fibrosis (Tefferi and Pardanani, 2015). Furthermore, of the Ph[−] MPNs, PMF has the most severe morbidity and greatest mortality, with the highest risk of leukemic transformation (Tefferi et al., 2014).

Ph[−] MPNs are clonal stem cell diseases united by the discovery of recurrent oncogenic driver mutations in *JAK2*, *CALR*, and *MPL* that lead to constitutive activation of the JAK–STAT signaling pathway (Baxter et al., 2005; James et al., 2005; Kralovics et al., 2005; Levine et al., 2005; Pikman et al., 2006; Klampfl et al., 2013; Nangalia et al., 2013). The advent

of clinically approved JAK inhibitors such as ruxolitinib to treat Ph[−] MPNs has shown promising results in ameliorating symptoms; however, it does not affect allele burden or significantly alter the course of disease (Tefferi, 2012; Tefferi and Pardanani, 2015). Whereas oncogenic *JAK2*, *CALR*, and *MPL* all play key roles in disease initiation (James et al., 2005; Pikman et al., 2006; Elf et al., 2016), there are many unknown cooperating molecular and genetic aberrations that contribute to disease pathogenesis. Furthermore, the determination of clonal hierarchy and temporal order of mutational occurrence in Ph[−] MPNs has proven complex (Tefferi, 2010). Recently, several mutations in epigenetic regulators (*IDH1/2*, *DNMT3A*, and *TET2*), signaling molecules (*SOCS*, *LNK*, and *CBL*), splicing factors (*SRSF2* and *SF3B1*), and even whole chromosomal rearrangements have been shown to precede driver mutation acquisition (Kralovics et al., 2006; Schaub et al., 2009, 2010; Wang et al., 2009; Abdel-Wahab et al., 2012; Tibes et al., 2012), highlighting the importance of these factors in contributing to Ph[−] MPN disease formation and pathogenesis. The identification and study of novel cellular and molecular mechanisms that contribute to Ph[−] MPN disease initiation is critical for understanding the molecular pathways that drive these diseases, and may also offer new opportunities for therapeutic intervention.

Nucleolar protein 3 (also known as apoptosis repressor with caspase recruitment domain [ARC]) is encoded by the

*R.F. Stanley and R.T. Piszczatowski contributed equally to this paper.

Correspondence to Ulrich Steidl: ulrich.steidl@einstein.yu.edu

Abbreviations used: AML, acute myeloid leukemia; AML-MRC, AML with myelodysplasia-related changes; ARC, apoptosis repressor with caspase recruitment domain; CMP, common myeloid progenitor; G-CSF, granulocyte-colony stimulating factor; GEO, Gene Expression Omnibus; GMP, granulocyte/monocyte progenitor; GSEA, Gene Set Enrichment Analysis; H&E, hematoxylin and eosin; LK, Lin[−]Sca-1⁺c-kit⁺; LSK, Lin[−]Sca-1⁺c-kit⁺; LT-HSC, long-term hematopoietic stem cell; MDS, myelodysplastic syndrome; MEP, megakaryocyte/erythrocyte progenitor; MPN, myeloproliferative neoplasm; MPP, multipotent progenitor; Ph, Philadelphia chromosome; PMF, primary myelofibrosis; SNP, single nucleotide polymorphism; ST-HSC, short-term hematopoietic stem cell; TPO, thrombopoietin; UPD, uniparental disomy.

© 2017 Stanley et al. This article is distributed under the terms of an Attribution–Noncommercial–Share Alike–No Mirror Sites license for the first six months after the publication date (see <http://www.rupress.org/terms/>). After six months it is available under a Creative Commons License (Attribution–Noncommercial–Share Alike 4.0 International license, as described at <https://creativecommons.org/licenses/by-nc-sa/4.0/>).



Nol3 gene and is highly expressed in cardiac and skeletal myocytes, neurons, and β -cells of the pancreas (Geertman et al., 1996; Koseki et al., 1998; McKimpson et al., 2013). In these tissues, ARC is a potent inhibitor of cell death and has the unique ability to antagonize both the intrinsic and extrinsic apoptosis pathways (Nam et al., 2004). ARC has been shown to have increased expression in solid tumors and in blast cells of patients with acute myeloid leukemia (AML), and to mediate cellular responsiveness to pharmacologic apoptosis induction (Wang et al., 2005; Mercier et al., 2008; Carter et al., 2011; Medina-Ramirez et al., 2011; Mak et al., 2014a,b). Interestingly, a recent study also revealed that ARC may play a tumor suppressor role in renal cell carcinoma cells, suggesting dual roles for ARC in oncogenesis that may be cell type-dependent (Gobe et al., 2016). Despite its name, NOL3/ARC primarily resides in the cytoplasm in most cell types, but was reported to localize to the nucleus in some solid tumor cell lines (Mercier et al., 2005; Wang et al., 2005). ARC protein has been reported to suppress NF- κ B pathway activation and to interact directly with p53 to disrupt its transcriptional activity in cancer cells (Foo et al., 2007; Kung et al., 2014). The role of ARC in normal and malignant hematopoiesis is largely unclear and has not yet been assessed using genetically engineered mouse models.

In this study, we investigated the functional and molecular consequences of loss of *Nol3*/ARC on the hematopoietic system. Unexpectedly, we found that *Nol3*^{-/-} mice develop a progressive MPN with features resembling PMF, including thrombocytopenia, anemia, extramedullary hematopoiesis, bone marrow fibrosis, and an expanded stem cell compartment. Moreover, we show that increased JAK-STAT activation in the expanded stem cell compartment leads to enhanced cell cycling and a myelomonocytic differentiation bias that is dependent on CDK6 and Myc activation. Furthermore, we find that the *Nol3*^{-/-} MPN phenotype shares significant molecular similarities with CD34⁺ cells from patients with PMF. Additionally, *NOL3* levels are decreased in CD34⁺ cells of patients with PMF, and *NOL3* is deleted in a subset of patients with myeloid malignancies. Our study provides a novel PMF-like mouse model with similarities to human PMF, implicates *Nol3* as a negative modulator of JAK-STAT signaling, and reveals a tumor suppressor role for *NOL3* in the pathogenesis of myeloid malignancies.

RESULTS

Loss of *Nol3* leads to peripheral cytopenias and extramedullary hematopoiesis

Loss of ARC protein expression in *Nol3*-null mice (*Nol3*^{-/-}) was confirmed by Western blot analysis of heart tissue and bone marrow cells (Fig. S1, A and B). ARC is expressed in total bone marrow cells from *Nol3*^{+/+} mice and purification into mature lineage positive (Lin⁺) and immature (Lin⁻cKit⁺) cells markedly enriched for ARC expression in the immature bone marrow fraction (Fig. S1 B). Consistent with this, qPCR analysis of wild-type animals showed low or absent *Nol3* tran-

script expression in sorted B cells, T cells, erythrocyte precursors, and mature myeloid blood cells; however, we detected elevated expression in the Lin⁻Sca-1⁺cKit⁺ (LSK) stem and progenitor cell compartment. Further purification of stem cell populations based on FLK2 and THY1 expression showed stable *Nol3* expression in multipotent progenitor cells (MPPs; Lin⁻Sca-1⁺cKit⁺Flk2⁺Thy1⁻), short-term hematopoietic stem cells (ST-HSCs; Lin⁻Sca-1⁺cKit⁺Flk2⁺Thy1⁺), and long-term HSCs (LT-HSCs; Lin⁻Sca-1⁺cKit⁺Flk2⁻Thy1⁺; Fig. S1 C).

Peripheral blood analysis of 11–18-mo-old *Nol3*^{-/-} mice showed anemia and thrombocytopenia, as well as significant increases in peripheral blood monocyte and neutrophil percentages with a decrease in lymphocyte percentage in comparison to age-matched *Nol3*^{+/+} mice (Fig. 1 A and Table S1). This phenotype was detectable in ~20% of *Nol3*^{-/-} analyzed mice. Strikingly, these mice displayed significant splenomegaly (>200 mg) and increased spleen cell number compared with *Nol3*^{+/+} mice (Fig. 1, B and C; and Fig. S1 D). Hematoxylin and eosin (H&E) staining of *Nol3*^{-/-} spleens revealed severely disordered splenic architecture, including disruption of lymphoid follicles, an infiltration of larger cells, and megakaryocyte hyperplasia and clustering, which is a hallmark of MPN (Fig. 1 D). Additionally, *Nol3*^{-/-} spleens showed increased staining for myeloperoxidase, indicative of active splenic myelopoiesis (Fig. 1 E). Interestingly, no significant difference in the percentage of apoptotic spleen cells in *Nol3*^{+/+} and *Nol3*^{-/-} mice was observed (Fig. S1 E). Additionally, hematopoietic cell infiltration was present in the livers of *Nol3*^{-/-} mice (Fig. S1 F). To determine if cells in *Nol3*^{-/-} spleens were actively proliferating, we stained spleen cells with Hoechst 33342 and detected a significant increase in the percentage of cells in the S-G2/M phase of the cell cycle compared with *Nol3*^{+/+} (Fig. 1, F and G). We next used flow cytometry to identify the expanded cell types in *Nol3*^{-/-} spleens and detected significant increases in the absolute number of almost all mature cell types analyzed, including granulocytes (Gr-1⁺CD11b⁺), erythrocyte precursors (Ter119⁺CD71⁺), megakaryocytes (CD41⁺), B cells (B220⁺), and T cells (CD3e⁺; Fig. 1 H). Elevation of numbers of myelo-erythroid cells correlated with overall spleen weight. We also observed significant increases in immature LK (Lin⁻Sca-1⁻cKit⁺) and LSK cells in the spleen (Fig. 1 I). Collectively, these findings are consistent with active extramedullary hematopoiesis in the spleens of *Nol3*^{-/-} mice.

Myeloproliferation and myelofibrosis in the bone marrow of *Nol3*^{-/-} mice

Investigation of femurs from *Nol3*^{-/-} animals showed a macroscopically pale appearance, and cell counts revealed a reduction in total bone marrow, including both myeloid and lymphoid cell populations compared with *Nol3*^{+/+} mice (Fig. 2, A–C). H&E staining of femur sections showed a reduction in blood sinusoids and significant reticulin staining, a marker of bone marrow fibrosis that is frequently found in patients with PMF (Fig. 2, D and E). Cell cycle analysis

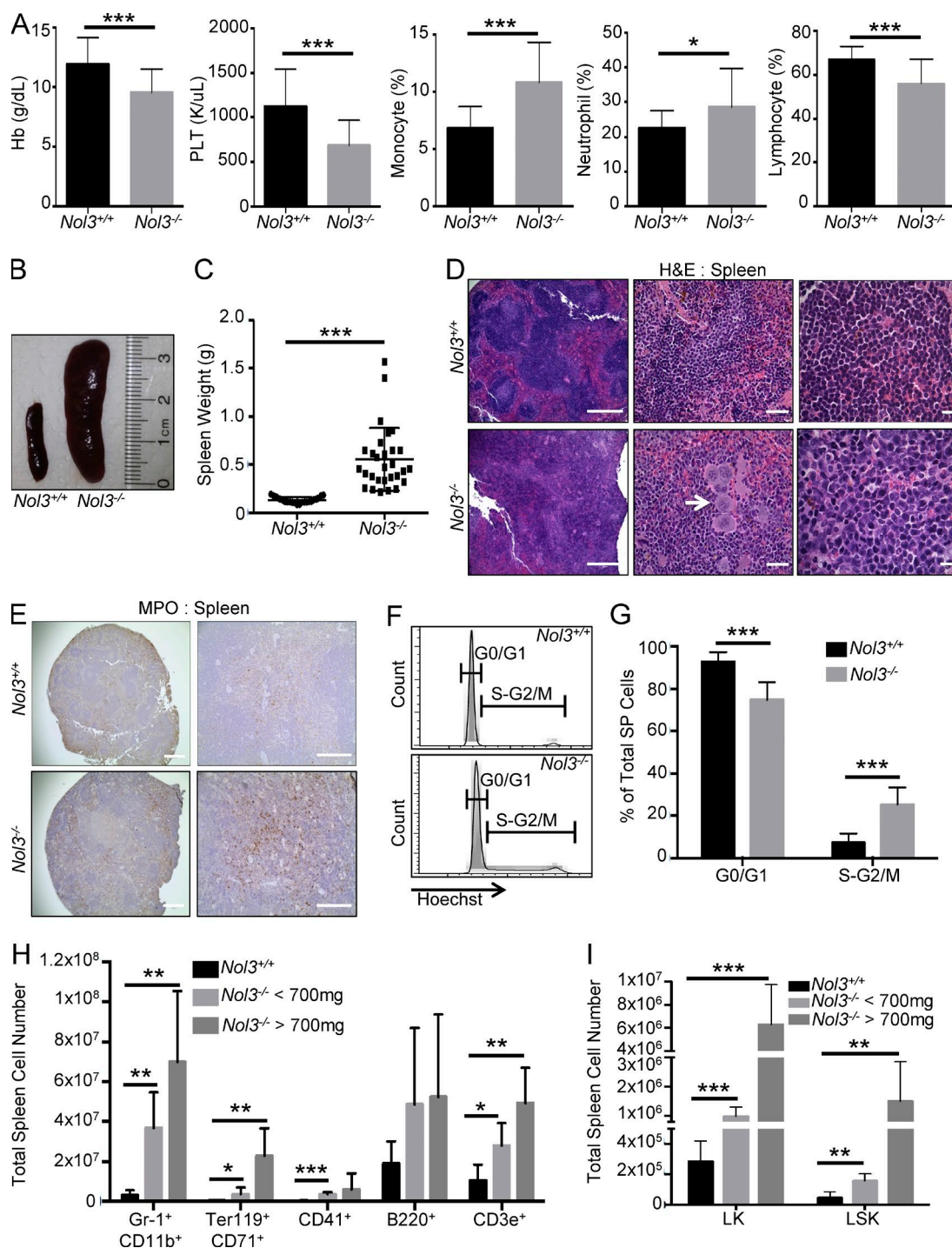


Figure 1. *Nol3* deletion leads to peripheral cytopenias and extramedullary hematopoiesis. (A) Hemoglobin (Hb), platelet count (PLT), monocyte, neutrophil, and lymphocyte percentage in the peripheral blood of *Nol3^{+/+}* and *Nol3^{-/-}* mice (*Nol3^{+/+}*, n = 20; *Nol3^{-/-}*, n = 25). (B) Representative images of spleens from *Nol3^{+/+}* and *Nol3^{-/-}* mice. (C) Spleen weights of *Nol3^{+/+}* and *Nol3^{-/-}* mice (*Nol3^{+/+}*, n = 23; *Nol3^{-/-}*, n = 29). (D) H&E staining of *Nol3^{+/+}* and *Nol3^{-/-}* spleens. White arrow highlights megakaryocyte clustering in *Nol3^{-/-}* spleens. Bars: (left) 400 μ m; (middle) 80 μ m; (right) 10 μ m. (E) Representative images of myeloperoxidase staining of *Nol3^{+/+}* and *Nol3^{-/-}* spleens. Bars: (left) 1,000 μ m; (right) 200 μ m. (F and G) Representative histogram plots and quantification of Hoechst-stained spleen cells for cell cycle analysis of *Nol3^{+/+}* and *Nol3^{-/-}* spleens (*Nol3^{+/+}*, n = 7; *Nol3^{-/-}*, n = 5). (H) Total cell numbers of mature cells of different lineages in *Nol3^{+/+}* and *Nol3^{-/-}* spleens (*Nol3^{+/+}*, n = 6; *Nol3^{-/-}* < 700 mg spleen weight, n = 5; *Nol3^{-/-}* > 700 mg spleen weight, n = 3). (I) Total cell numbers of LK and LSK cells in *Nol3^{+/+}* and *Nol3^{-/-}* spleens (*Nol3^{+/+}*, n = 7; *Nol3^{-/-}* < 700 mg spleen weight, n = 4; *Nol3^{-/-}* > 700 mg spleen weight, n = 2). Bars represent mean values. Error bars represent \pm SD; *, P < 0.05; **, P < 0.01; ***, P < 0.001.

of *Nol3*^{-/-} bone marrow cells showed a significant increase in the percentage of cells in the S-G2/M phase of the cell cycle compared with *Nol3*^{+/+} cells (Fig. 2, F and G). As in the spleen, comparison of *Nol3*^{+/+} and *Nol3*^{-/-} cells in the bone marrow showed no significant difference in the percentage of cells undergoing apoptosis, suggesting that ARC may not be essential to apoptosis inhibition in hematopoietic cells (Fig. 2 H; also see Fig. S1 E).

The abnormal peripheral blood counts, extramedullary hematopoiesis with megakaryocyte hyperplasia and clustering, increased cell proliferation, and presence of bone marrow fibrosis in *Nol3*^{-/-} mice are features consistent with an MPN phenotype that resembles PMF (now termed *Nol3*^{-/-} MPN). Congruous with this PMF-like phenotype, we observed a significant increase in colony formation from peripheral blood cells of *Nol3*^{-/-} MPN mice, indicative of increased circulating stem and progenitor cells, which is frequently observed in patients with PMF (Fig. 2 I; Andréasson et al., 2002). In addition, it has been shown that aberrant expression and activity of cytokines plays an integral role in the pathogenesis of MPNs and PMF. To identify cytokines involved in *Nol3*^{-/-} MPN, we profiled the serum of *Nol3*^{+/+} and *Nol3*^{-/-} MPN mice and found a significant increase in circulating granulocyte-colony stimulating factor (G-CSF), as well as elevated circulating IL-1-β (Fig. 2 J), both of which have been previously implicated in the pathogenesis of human PMF (Tefferi et al., 2011).

***Nol3*^{-/-}-induced MPN is intrinsic to hematopoietic cells and transplantable to irradiated congenic recipients**

To determine whether the MPN observed in *Nol3*^{-/-} mice was intrinsic to hematopoietic cells, we transplanted total bone marrow cells from *Nol3*^{+/+} and *Nol3*^{-/-} MPN (CD45.2⁺) mice into lethally irradiated CD45.1⁺ wild-type recipients. At 6–8 mo after transplantation all recipient mice were sacrificed for detection of donor-derived disease. All recipient mice evaluated for MPN initiation had >93% donor cell chimerism in the peripheral blood at time of sacrifice (Fig. S1 G). Transplantation of bone marrow from 11 individual *Nol3*^{-/-} MPN mice resulted in four recipient mice (36.4%) developing donor-derived disease, whereas no *Nol3*^{+/+} recipients developed MPN. The MPN phenotype in *Nol3*^{-/-} recipient mice was indistinguishable from the MPN in donor mice, with pale femurs, splenomegaly, decreased platelet counts, and increased monocyte counts in the peripheral blood, in comparison to *Nol3*^{+/+} cell recipients (Fig. 3, A–D). In addition, H&E and reticulin staining showed reduced blood sinuses and increased reticulin staining in the bone marrow, as well as severely disorganized splenic architecture, including disruption of lymphoid follicles and clustering of megakaryocytes, further confirming the MPN phenotype in recipient mice (Fig. 3, E–G). Interestingly, congenic transplantation of total spleen cells from three individual *Nol3*^{-/-} MPN mice also generated donor-derived MPN in two recipient mice (66.6%) at time of sacrifice, indicating that disease-initiating cells of *Nol3*^{-/-}

MPN are present and transplantable from either hematopoietic compartment (Fig. 3 H and Fig. S1 H).

To determine whether *Nol3*^{-/-} MPN bone marrow cells have a competitive advantage, we performed competitive repopulation transplantation assays and found that *Nol3*^{-/-} MPN outcompeted *Nol3*^{+/+} bone marrow cells in recipient mice at 12 and >20 wk after transplantation (Fig. 3 I). Consistent with this, mice that received *Nol3*^{-/-} MPN marrow had significantly larger spleens and higher amounts of pale bone marrow compared with mice that received *Nol3*^{+/+} marrow, suggesting that *Nol3*^{-/-} MPN bone marrow cells exhibit increased self-renewal capacity compared with *Nol3*^{+/+} cells in vivo (Fig. S1, I and J). Interestingly, competitive stem cell transplantation experiments revealed no significant difference in engraftment between sorted *Nol3*^{+/+} and *Nol3*^{-/-} MPN stem cell populations at 16 wk after transplantation (Fig. S1 K), suggesting that the competitive advantage of *Nol3*^{-/-} MPN bone marrow cells is caused by the expansion of immature cellular subsets rather than increased self-renewal of individual stem cells.

Although there is strong evidence that MPNs are clonal stem cell diseases (Adamson et al., 1976; Jacobson et al., 1978; Fialkow et al., 1981), a possible involvement of bone marrow stromal cells in MPN disease pathogenesis has been suggested in several mouse models (Walkley et al., 2007a,b; Zimmer et al., 2011). To determine if nonhematopoietic stromal cell populations of *Nol3*^{-/-} mice can induce the MPN phenotype, we performed reciprocal transplantation experiments. Congenic FACS-purified wild-type CD45.1⁺ cells were transplanted into 3-mo-old lethally irradiated *Nol3*^{+/+} (*n* = 6) or *Nol3*^{-/-} (*n* = 13) CD45.2⁺ mice and sacrificed 11–12 mo after transplantation. There were no significant differences in spleen size or peripheral blood counts in *Nol3* experimental mice with >65% donor cell engraftment, and 0/13 *Nol3*^{-/-} recipient mice developed donor-derived disease (Figs. S1, L and M; and Table S1). Collectively, these results support a hematopoietic cell-intrinsic process in which the *Nol3*^{-/-} MPN is induced by deletion of *Nol3* in hematopoietic cells and can be recapitulated in transplantation experiments in congenic mice.

Hematopoietic stem and progenitor cells of *Nol3*^{-/-} MPN mice show active proliferation and a myelomonocytic differentiation bias

Investigation of hematopoietic stem and progenitor cell compartments by FACS revealed an increase in the percentage of LSK cells in *Nol3*^{-/-} MPN mice compared with *Nol3*^{+/+} mice but no significant changes in phenotypically defined myeloid progenitor subpopulations (Fig. 4, A–D). Further analysis of the LSK population revealed a decrease in the percentage of MPPs but an increase in ST- and LT-HSCs (Fig. 4 E). Overall, there was a significant expansion in the percentage of Thy1⁺ LSK cells in *Nol3*^{-/-} MPN mice (Fig. 4, B and E). To verify an expanded stem cell population in the setting of an overall reduction in total bone marrow cellularity in *Nol3*^{-/-} MPN (Fig. 2 B), we determined absolute

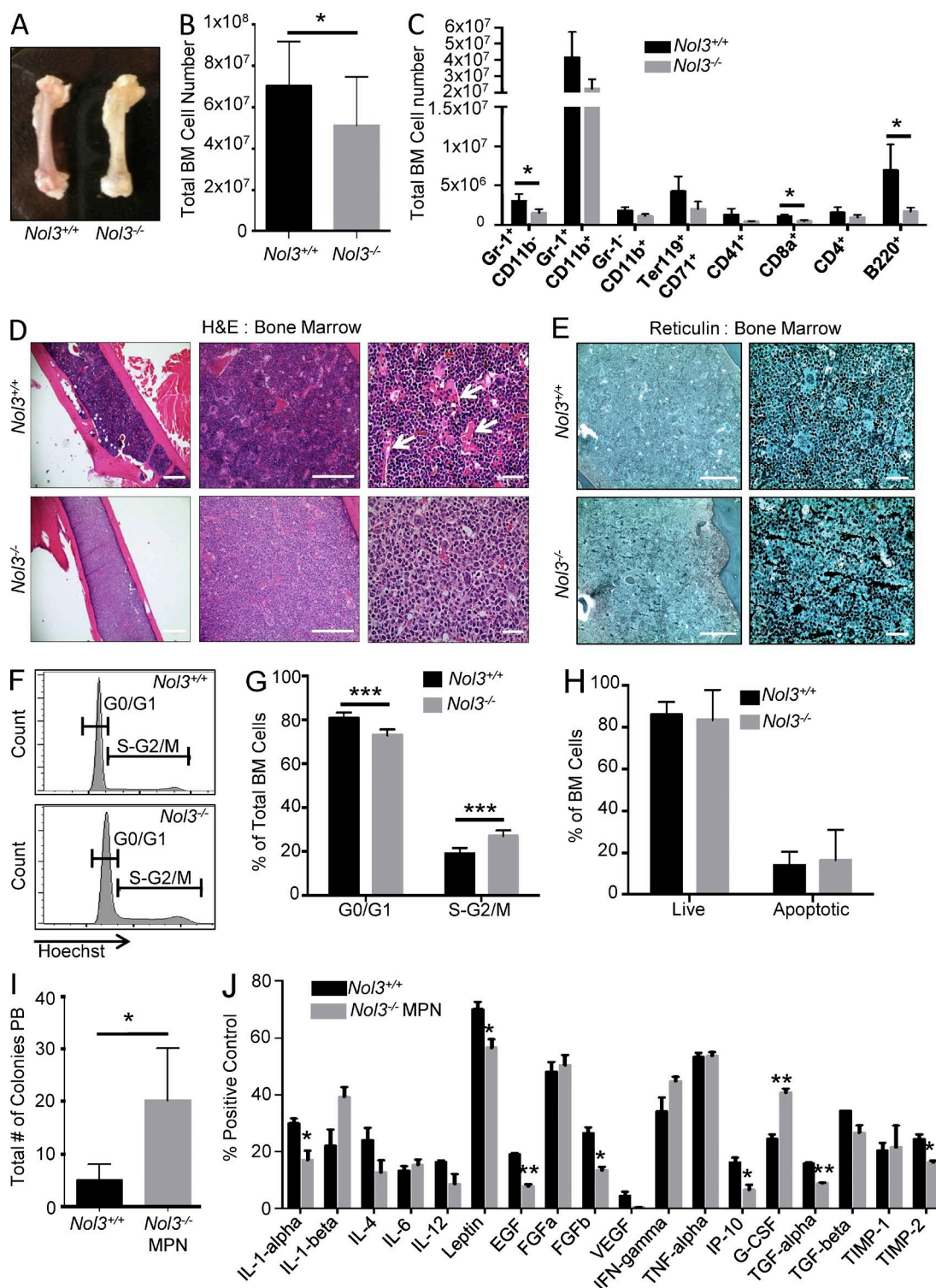


Figure 2. Increased proliferation and myelofibrosis in *NOL3*^{-/-} bone marrow. (A) Representative femurs from *NOL3*^{+/+} and *NOL3*^{-/-} mice. (B) Total number of cells in *NOL3*^{+/+} and *NOL3*^{-/-} bone marrow (*NOL3*^{+/+}, *n* = 17; *NOL3*^{-/-}, *n* = 10). (C) Absolute number of mature cell types in *NOL3*^{+/+} and *NOL3*^{-/-} bone marrow (*NOL3*^{+/+}, *n* = 4; *NOL3*^{-/-}, *n* = 5). (D) H&E staining of *NOL3*^{+/+} and *NOL3*^{-/-} bone marrow sections. Arrows highlight blood sinusoids present in *NOL3*^{+/+} femurs. Bars: (left) 1,000 μ m; (middle) 200 μ m; (right) 80 μ m. (E) Reticulin staining of *NOL3*^{+/+} and *NOL3*^{-/-} bone marrow sections. Bars: (left) 200 μ m; (right) 80 μ m. (F and G) Representative histogram plots and quantification of Hoechst stained bone marrow cells for cell cycle analysis of *NOL3*^{+/+} and *NOL3*^{-/-} bone marrow (*NOL3*^{+/+}, *n* = 7; *NOL3*^{-/-}, *n* = 5). (H) Percentage of live and apoptotic cells in the bone marrow of *NOL3*^{+/+}

numbers of stem and progenitor cells. We found a statistically significant increase in the absolute numbers of ST- and LT-HSC, as well as Thy1⁺LSK cells, with no change in the absolute numbers of progenitor cell populations (Fig. 5, A and B). Notably, absolute numbers of MPP, ST-HSC, LT-HSC, and Thy1⁺LSK cells were also elevated in spleens of *Nol3*^{-/-} MPN mice (Fig. 5 C).

To investigate the cell biological phenotype of the expanded Thy1⁺LSK cells, we performed cell cycle analysis using Hoechst 33342 and the proliferation marker Ki67. *Nol3*^{-/-} MPN Thy1⁺LSK cells showed significantly increased cell cycling compared with *Nol3*^{+/+} Thy1⁺LSK cells (Fig. 5, D and E). Remarkably, analysis of the percentage of apoptotic cells showed no significant difference between *Nol3*^{+/+} and *Nol3*^{-/-} MPN Thy1⁺LSK cells as well as LK or LSK cells (Fig. 5, F–H). Methylcellulose colony assays demonstrated a commitment bias toward myeloid colony formation, with a significant increase in the percentage of CFU-M (monocyte) over CFU-E (erythroid) colonies from *Nol3*^{-/-} MPN Thy1⁺LSK cells compared with *Nol3*^{+/+} Thy1⁺LSK control cells (Fig. 5 I). FACS analysis of colony assay cells showed a significant increase in the percentage of Gr-1⁺CD11b⁺ monocytic cells derived from *Nol3*^{-/-} MPN Thy1⁺LSK cells, which was also evident by morphological analysis after May–Grünwald Giemsa staining (Fig. 5, J–L).

JAK–STAT signaling is activated in stem and progenitor cells in *Nol3*^{-/-} MPN, and *Cdk6* and *Myc* are functionally relevant downstream targets

To obtain insight into the molecular consequences of *Nol3* deletion in the expanded Thy1⁺LSK cell population, we performed gene expression profiling on FACS sorted *Nol3*^{+/+} and *Nol3*^{-/-} MPN Thy1⁺LSK cells (complete data available in Gene Expression Omnibus [GEO] under accession no. GSE76121). Gene set enrichment analysis (GSEA) identified significant enrichment of STAT5 and STAT3 gene signaling pathways in *Nol3*^{-/-} MPN compared with *Nol3*^{+/+} Thy1⁺LSK cells, suggesting JAK–STAT signaling involvement in *Nol3*^{-/-} MPN (Fig. 6 A). We performed phospho-flow cytometry experiments of stem and progenitor cells and indeed found significant activation of pSTAT5 and pSTAT3 in *Nol3*^{-/-} MPN bone marrow LK and LSK cells, demonstrating activation of JAK–STAT signaling in the *Nol3*^{-/-} MPN model (Fig. 6, B–G). Western blot analysis confirmed increased activation of pSTAT3 in spleen cells from *Nol3*^{-/-} MPN (Fig. 6 H). Notably, increased pSTAT5 and pSTAT3 activation in *Nol3*^{-/-} MPN cells was also seen upon stimulation with thrombopoietin (TPO) and G-CSF (Fig. 6, B–H), cytokines that have been implicated in PMF and act on JAK–STAT signaling pathways (Oh et al., 2010; Tefferi et al., 2011).

Further investigation of differentially expressed genes by GSEA uncovered signatures known to be downstream of JAK–STAT signaling that reflect the cellular phenotypes observed in *Nol3*^{-/-} MPN Thy1⁺LSK cells, including cell cycle and *Myc* target signatures, as well as genes up-regulated in monocytic differentiation (Fig. 7 A). STAT5 and STAT3 have previously been shown to activate *Myc* and cell cycle regulators, including *Cdk6* (Fukada et al., 1998; Kiuchi et al., 1999; Lin et al., 2012; Pinz et al., 2016). We validated *Cdk6* and *Myc* up-regulation in *Nol3*^{-/-} MPN Thy1⁺LSK cells by qRT-PCR (Fig. 7 B). To test whether the increase in *Cdk6* and *Myc* expression in *Nol3*^{-/-} MPN LSK cells is functionally relevant, we treated *Nol3*^{-/-} MPN LSK cells with two different small molecule inhibitors targeted toward these pathways and assessed colony formation capacity. Palbociclib is a CDK4/6 inhibitor that causes sustained cell cycle arrest (Fry et al., 2004) and JQ1 is a bromodomain/BRD4 inhibitor that causes repression of *Myc* transcription (Delmore et al., 2011). Strikingly, inhibition of CDK4/6 or *Myc* resulted in rescue of the myeloid bias observed in *Nol3*^{-/-} MPN cells (Fig. 7, C and D). These data indicate that the *Nol3*^{-/-}-induced phenotype in the immature stem cell population is, at least in part, mediated by activation of CDK4/CDK6 and *Myc*.

NOL3 is functionally relevant in human PMF cells and frequently down-regulated in CD34⁺ cells of PMF patients, and deletions of the *NOL3* locus are found in patients with myeloid malignancies

To interrogate the functional significance of *NOL3*/ARC in human MPN cells, we ectopically re-expressed ARC protein in HEL cells (which carry a deletion of the *NOL3* locus), as well as SET-2 and UKE-1 cell lines. Ectopic expression of ARC protein led to a significant reduction in colony formation and inhibition of the JAK–STAT signaling pathway in all three cell lines compared with lentiviral vector control cells (Fig. 8, A and B). Additionally, colony formation capacity of all three cell lines was significantly inhibited with CDK4/6 inhibitor treatment (Fig. 8 C). These results implicate ARC as a negative modulator of JAK–STAT signaling and as functionally relevant in human MPN.

To interrogate whether the molecular alterations seen in the *Nol3*^{-/-} MPN mouse model resemble human PMF, we analyzed gene expression data of isolated CD34⁺ cells from PMF patients (available in GEO under accession no. GSE53482; Norfo et al., 2014). Investigation of *NOL3* mRNA expression in the context of human PMF (accession no. GSE53482) revealed a significant reduction in *NOL3* expression in CD34⁺ cells from the majority of PMF patients compared with healthy control cells (Fig. 9, A and B). Interestingly, *NOL3* expression was significantly decreased

and *Nol3*^{-/-} mice measured by Annexin V and DAPI staining ($n = 6$). (I) Peripheral blood colony assay of *Nol3*^{+/+} and *Nol3*^{-/-} MPN mice (*Nol3*^{+/+}, $n = 5$; *Nol3*^{-/-} MPN, $n = 4$). (J) Cytokine measurements from pooled serum samples of *Nol3*^{+/+} or *Nol3*^{-/-} mice ($n = 6$). Bars represent mean values. Error bars represent \pm SD; *, $P < 0.05$; **, $P < 0.01$; ***, $P < 0.001$.

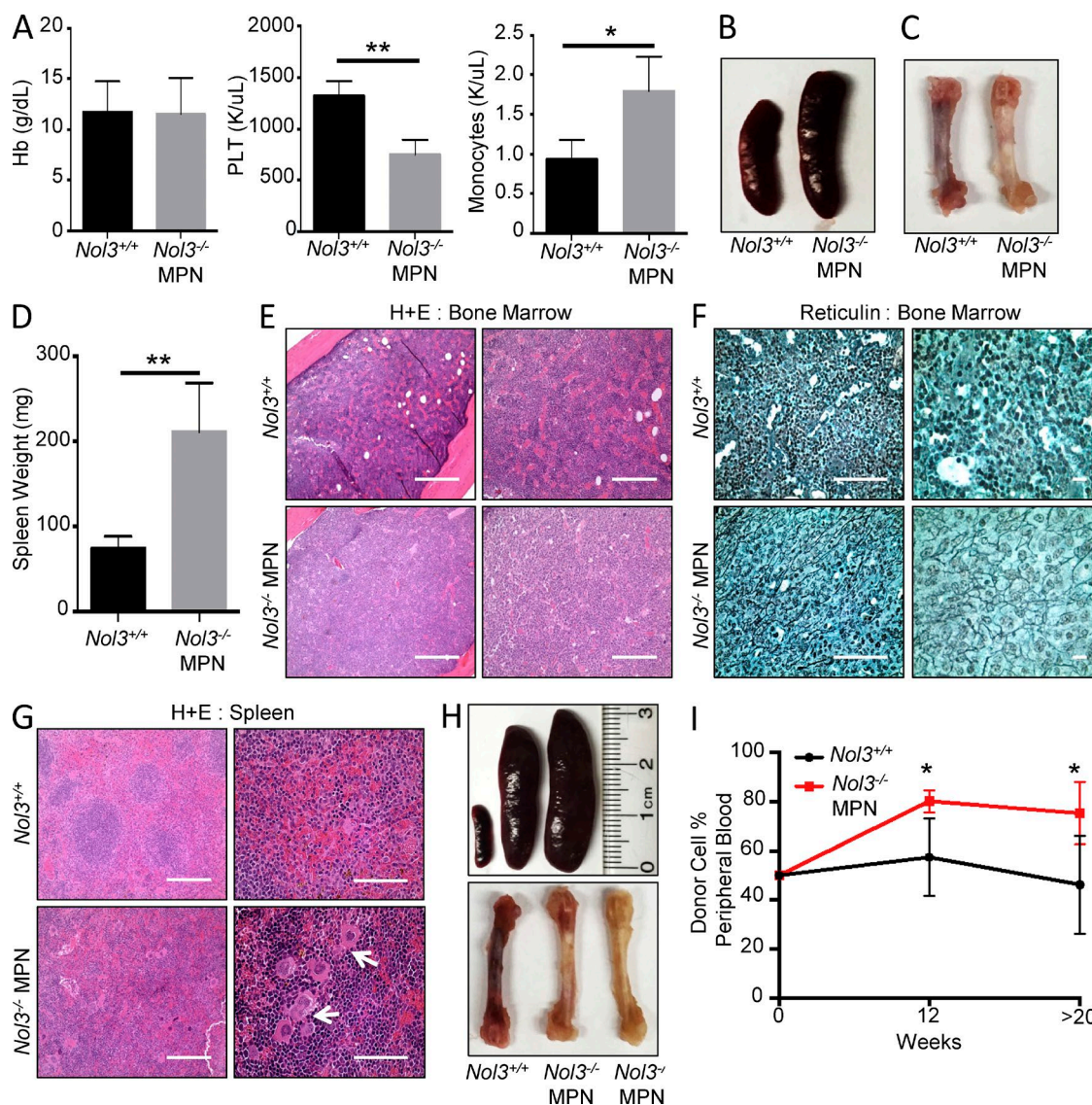


Figure 3. *Nol3*^{-/-}-induced MPN is cell intrinsic and transplantable into congenic recipients. (A) Peripheral blood counts of mice transplanted with either *Nol3*^{+/+} or *Nol3*^{-/-} MPN whole bone marrow cells. Hemoglobin (Hb), platelet (PLT), and monocyte counts are shown ($n = 4$). (B and C) Representative spleen and bone marrow images of recipient mice after transplantation with *Nol3*^{+/+} or *Nol3*^{-/-} MPN total bone marrow cells. (D) Spleen weight of mice transplanted with either *Nol3*^{+/+} or *Nol3*^{-/-} MPN cells ($n = 4$). (E) Representative H&E of bone marrow sections from congenic recipient mice after transplantation with *Nol3*^{+/+} or *Nol3*^{-/-} MPN whole bone marrow cells. Bars: (left) 400 μ m; (right) 200 μ m. (F) Representative reticulin staining of bone marrow sections from congenic recipient mice after transplantation with *Nol3*^{+/+} or *Nol3*^{-/-} MPN whole bone marrow cells. Bars: (left) 80 μ m; (right) 10 μ m. (G) Representative H&E staining of spleen sections from congenic recipient mice after transplantation with *Nol3*^{+/+} or *Nol3*^{-/-} MPN cells. White arrows highlight megakaryocyte clustering in mice transplanted with *Nol3*-deficient cells. Bars: (left) 200 μ m; (right) 80 μ m. (H) Images of spleen and femoral bones of congenic recipient mice after transplantation with *Nol3*^{+/+} and *Nol3*^{-/-} MPN total spleen cells. (I) Percentage of peripheral blood donor cell engraftment at 12 and >20 wk after competitive transplantation of either *Nol3*^{+/+} or *Nol3*^{-/-} cells with wild-type competitor cells (*Nol3*^{+/+}, $n = 6$; *Nol3*^{-/-} MPN, $n = 5$). Bars represent mean values. Error bars represent \pm SD; *, $P < 0.05$; **, $P < 0.01$.

compared with healthy controls regardless of the absence (JAK2WT) or presence of JAK2V617F mutations and there was no significant difference between these two mutational groups (Fig. 9, C and D).

Comparative GSEA analysis of differentially expressed gene sets in *Nol3*^{-/-} MPN Thy1⁺LSK cells (relative to age-

matched *Nol3*^{+/+} controls) identified overlapping gene sets that are also enriched in human CD34⁺ cells from patients with PMF (in comparison to healthy controls). We found significant positive enrichment of 87 shared gene sets between murine *Nol3*^{-/-} MPN and human PMF cells (Fig. 9 E; FDR < 0.01; $P < 2.2 \times 10^{-16}$; odds ratio, 28.19), including en-

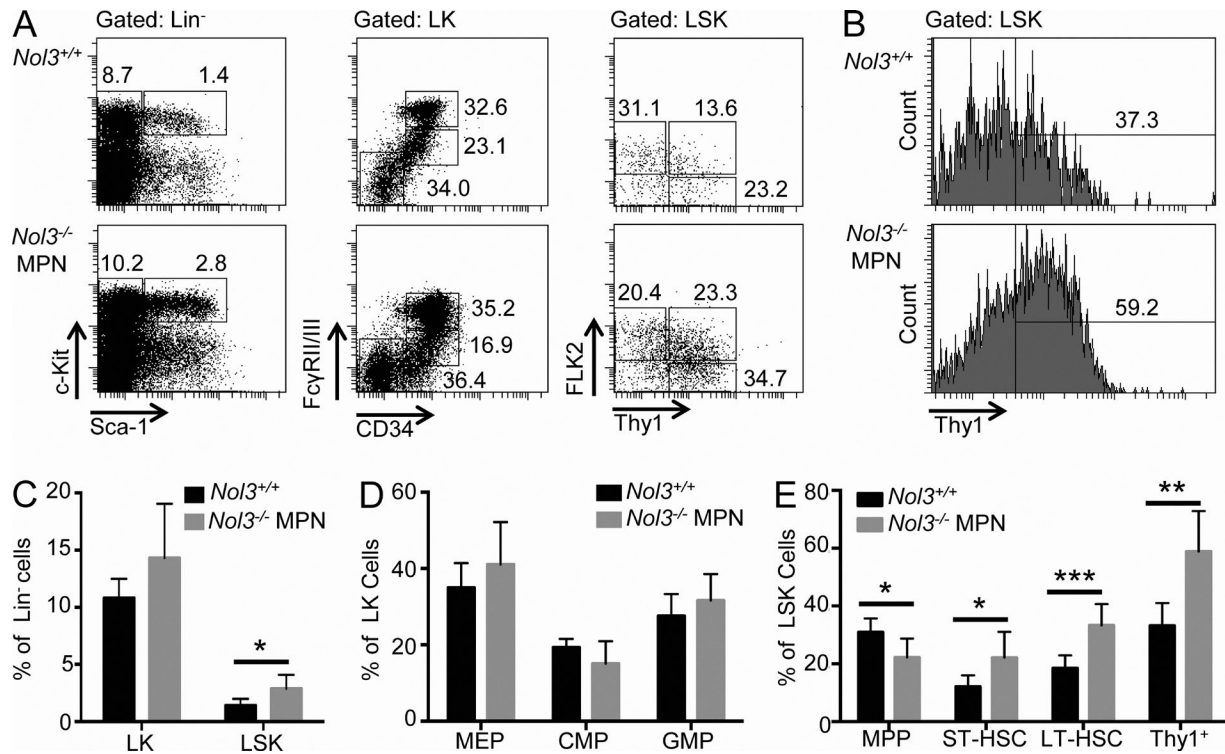


Figure 4. Increased stem cell populations in *NOL3*^{-/-} MPN mice. (A) Representative FACS plots of *NOL3*^{+/+} and *NOL3*^{-/-} MPN bone marrow cells. (left) Lineage⁻ bone marrow cells gated on c-Kit and Sca-1 to distinguish LK and LSK cells. (middle) LK cells co-stained with FcγRII/III and CD34 to distinguish common myeloid progenitor cells (CMPs; Lin⁻cKit⁺Sca-1⁻CD34⁺FcγRII/III^{lo}), granulocyte/monocyte progenitor cells (GMPs; Lin⁻cKit⁺Sca-1⁻CD34⁺FcγRII/III^{hi}), and megakaryocytic/erythroid progenitor cells (MEPs; Lin⁻cKit⁺Sca-1⁻CD34⁺FcγRII/III^{lo}). (right) LSK cells co-stained with FLK2 and THY1 to distinguish MPP, ST-HSC, and LT-HSC. Percentages of cell populations are indicated. (B) Histogram plot of Thy1⁺LSK cells from *NOL3*^{+/+} and *NOL3*^{-/-} MPN mice. (C) Percentage of LK and LSK cells in bone marrow of *NOL3*^{+/+} and *NOL3*^{-/-} MPN mice (*NOL3*^{+/+}, *n* = 7; *NOL3*^{-/-} MPN, *n* = 6). (D) Percentage of MEP, CMP, and GMP cells in bone marrow of *NOL3*^{+/+} and *NOL3*^{-/-} MPN mice (*NOL3*^{+/+}, *n* = 7; *NOL3*^{-/-} MPN, *n* = 6). (E) Percentage of MPP, ST-HSC, LT-HSC, and Thy1⁺LSK cells in bone marrow of *NOL3*^{+/+} and *NOL3*^{-/-} MPN mice (*NOL3*^{+/+}, *n* = 7; *NOL3*^{-/-} MPN, *n* = 6). Bars represent mean values. Error bars represent ±SD; *, *P* < 0.05; **, *P* < 0.01; ***, *P* < 0.001.

richment of gene sets involved in cell cycle regulation and MYC target gene expression. Furthermore, dichotomization of PMF patients into higher and lower *NOL3* expression showed a significant enrichment of 97 gene sets in *NOL3*-low expressing patients compared with *NOL3*^{-/-} MPN mice (Fig. 9 F; FDR < 0.01; *P* < 2.2 × 10⁻¹⁶; odds ratio, 27.99). Collectively, these findings show that the expanded Thy1⁺LSK cells in *NOL3*^{-/-} MPN share significant molecular features with CD34⁺ cells from patients with PMF.

To investigate whether deletion or loss of heterozygosity of *NOL3* occurs in human myeloid malignancies, we analyzed single nucleotide polymorphism (SNP) array data of patients with MPN, AML, chronic myelogenous leukemia, and myelodysplastic syndrome (MDS). We identified 17 patients (1.57% of all patients analyzed) with deletion or uniparental disomy (UPD) of *NOL3* (Fig. 9 G; for patient characteristics see Table S2). 7 of the 17 patients with *NOL3* deletion were diagnosed with AML with myelodysplasia-related changes (AML-MRC), an AML that occurs in patients with a previous history of MDS or MDS/MPN. For 7 out

of the 17 patients with *NOL3* deletion or UPD, diagnostic fibrosis data were available. Strikingly, five out of these seven patients were positive for bone marrow fibrosis (not depicted).

We also determined if *NOL3* expression is decreased in more stringently defined human hematopoietic stem cells from patients with myeloid malignancies. Microarray data from our laboratory revealed an ~30% reduction in *NOL3* mRNA expression in highly purified human LT-HSCs (Lin⁻CD34⁺CD38⁻CD90⁺) isolated from patients with AML with complex karyotype (three or more cytogenetic abnormalities) compared with age-matched healthy control cells (Fig. 9 H; Barreyro et al., 2012).

Collectively, these results support a role for *NOL3*, including at the HSC level in human MPN and other myeloid malignancies.

DISCUSSION

The discovery of oncogenic driver mutations that constitutively activate JAK-STAT signaling has been vital to understanding the pathophysiology of Ph⁻ MPNs. Targeting of the

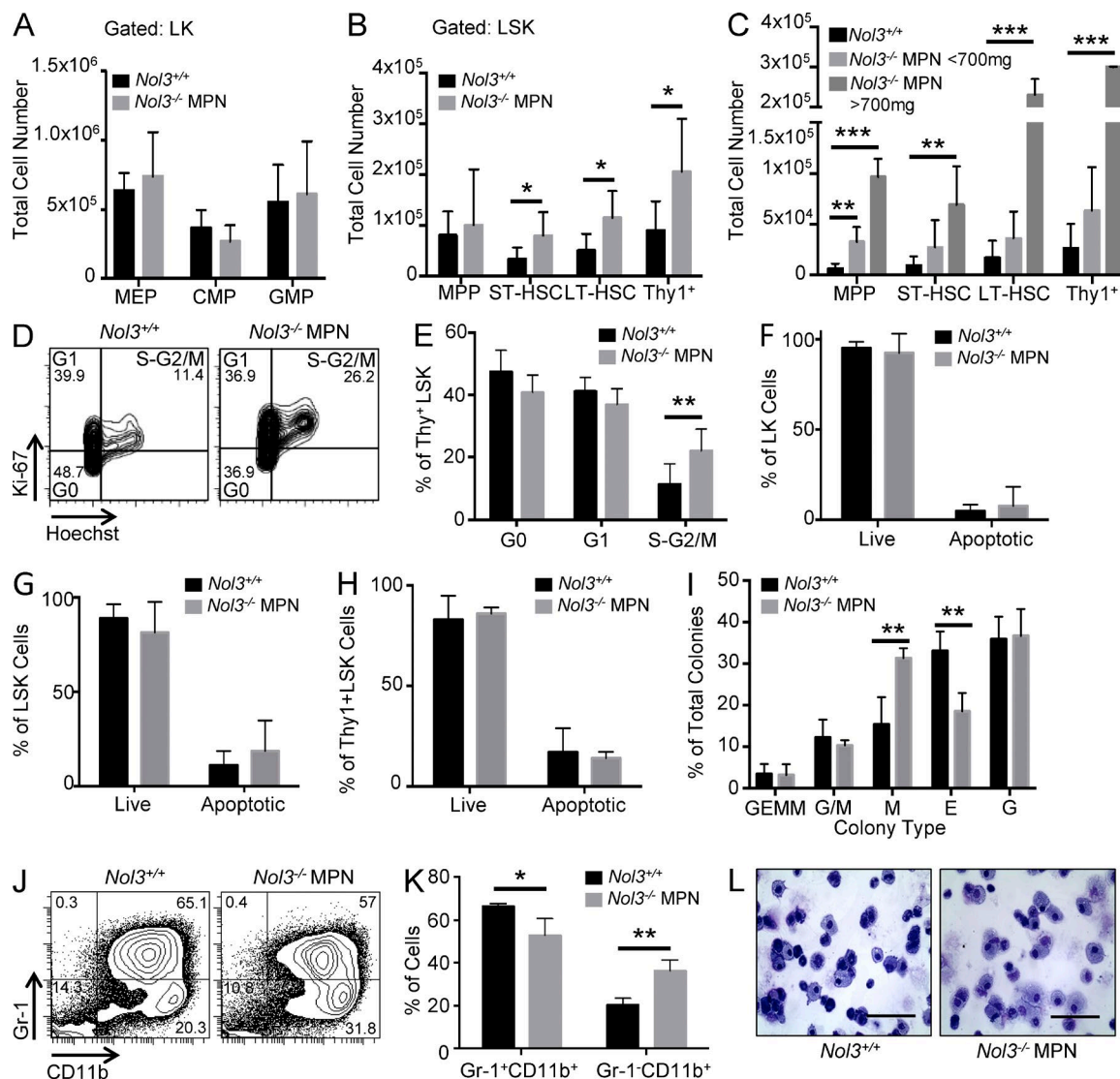


Figure 5. Expanded Thy1⁺LSK cells exhibit increased cycling and myeloid differentiation bias in *NOL3*^{-/-} MPN. (A) Absolute numbers of MEP, CMP, and GMP cells in bone marrow of *NOL3*^{+/+} and *NOL3*^{-/-} MPN mice (*NOL3*^{+/+}, *n* = 7; *NOL3*^{-/-} MPN, *n* = 6). (B) Absolute numbers of MPP, ST-HSC, LT-HSC, and Thy1⁺LSK cells in bone marrow of *NOL3*^{+/+} and *NOL3*^{-/-} MPN mice (*NOL3*^{+/+}, *n* = 7; *NOL3*^{-/-} MPN, *n* = 6). (C) Total cell number of MPP, ST-HSC, LT-HSC, and Thy1⁺LSK in spleens of *NOL3*^{+/+} and *NOL3*^{-/-} MPN mice (*NOL3*^{+/+}, *n* = 7; *NOL3*^{-/-} MPN < 700 mg, spleen, *n* = 4; *NOL3*^{-/-} MPN > 700 mg, spleen, *n* = 2). (D and E) Representative FACS plots and quantification of the cell cycle status of *NOL3*^{+/+} and *NOL3*^{-/-} MPN Thy1⁺LSK bone marrow cells based on Ki-67 and Hoechst staining (*NOL3*^{+/+}, *n* = 7; *NOL3*^{-/-} MPN, *n* = 8). (F–H) Percentage of live and apoptotic cells in bone marrow LK, LSK, and Thy1⁺LSK cells, respectively, from *NOL3*^{+/+} and *NOL3*^{-/-} MPN mice measured by Annexin V and DAPI staining (*n* = 3). (I) Colony-forming capacity of sorted *NOL3*^{+/+} and *NOL3*^{-/-} MPN Thy1⁺LSK (*NOL3*^{+/+}, *n* = 6; *NOL3*^{-/-} MPN, *n* = 3). (J) Representative FACS plots of Gr-1 and CD11b staining of colonies derived from *NOL3*^{+/+} and *NOL3*^{-/-} MPN cells. (K) Percentage of Gr-1⁺CD11b⁺ and Gr-1⁻CD11b⁺ cells after colony formation assay of *NOL3*^{+/+} and *NOL3*^{-/-} MPN cells (*n* = 3). (L) Wright-Giemsa staining of cytopun cells after colony assay of *NOL3*^{+/+} and *NOL3*^{-/-} MPN Thy1⁺LSK cells. Bars, 80 μ m. Bars represent mean values. Error bars represent \pm SD; *, *P* < 0.05; **, *P* < 0.01; ***, *P* < 0.001.

JAK–STAT pathway has shown promising results in alleviating symptoms; however, it has not significantly altered the course of disease, suggesting that additional underlying factors play key roles in Ph⁻ MPN pathophysiology.

Our results show that *NOL3* is primarily expressed in hematopoietic stem and progenitor cells and that loss of *NOL3* in mice confers phenotypic and molecular similarities to human

PMF. *NOL3*^{-/-} MPN mice develop an expanded Thy1⁺LSK stem cell population that exhibits functional alterations in cell cycling, as well as a bias toward myelomonocytic differentiation. Cytokines play a major role in the pathogenesis of PMF, and our results show elevated levels of circulating G-CSF in *NOL3*^{-/-} MPN mice. Furthermore, *NOL3*^{-/-} MPN stem cells show increased activation of JAK–STAT signaling in response

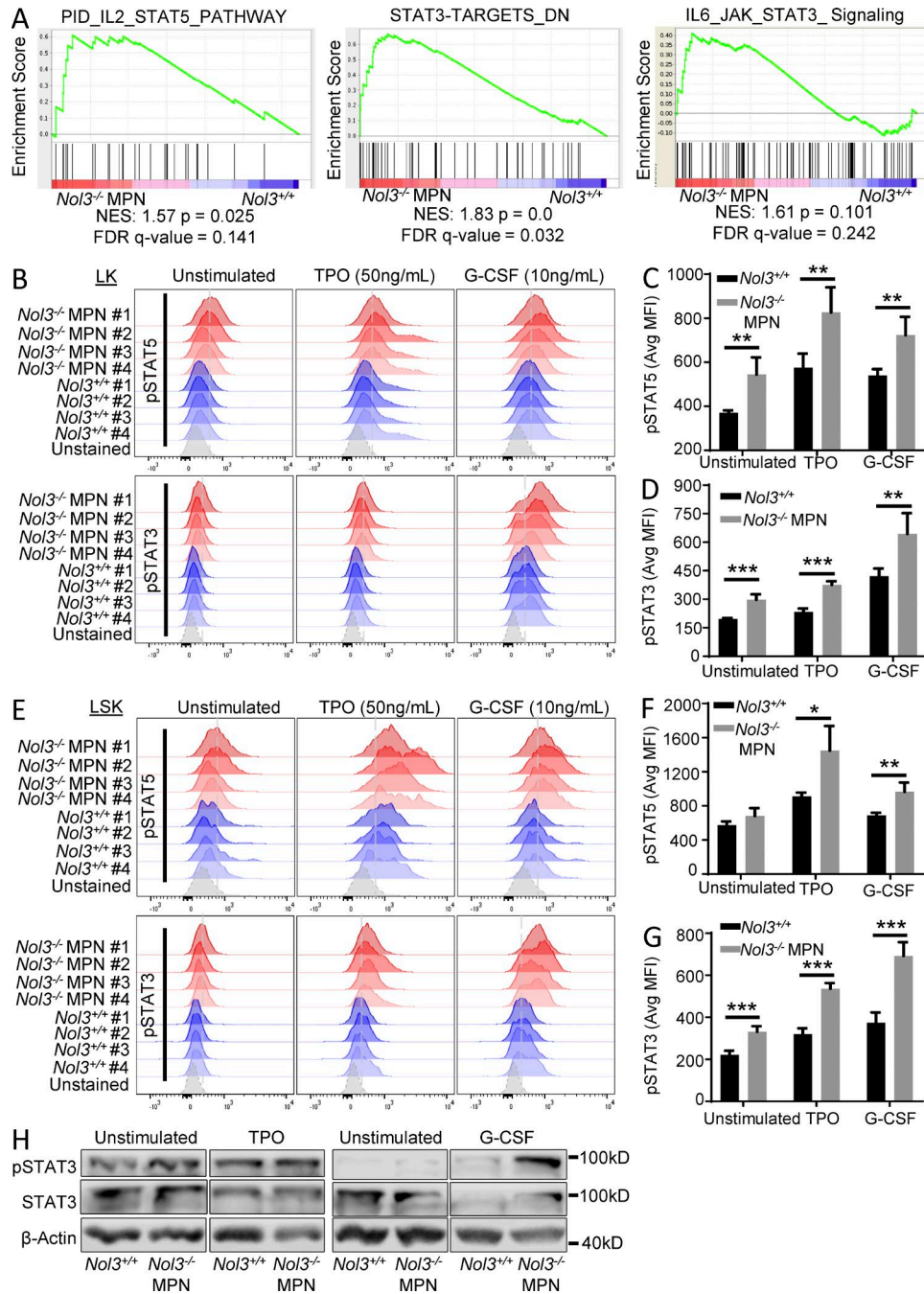


Figure 6. ***Nol3*-deficient stem and progenitor cells show increased JAK-STAT activation.** (A) GSEA of pathways enriched in *Nol3*^{-/-} MPN Thy1⁺LSK cells compared with *Nol3*^{+/+} Thy1⁺LSK cells. (B) Phospho-flow analysis of pSTAT5 and pSTAT3 in LK cells of *Nol3*^{+/+} and *Nol3*^{-/-} MPN mice, under unstimulated, TPO-stimulated (50 ng/ml), and G-CSF-stimulated (10 ng/ml) conditions (*n* = 4). (C and D) Quantification of phospho-flow analysis of pSTAT5 and pSTAT3, respectively, in LK cells from *Nol3*^{+/+} and *Nol3*^{-/-} MPN mice (MFI, mean fluorescence intensity; *n* = 4). (E) Phospho-flow analysis of pSTAT5 and pSTAT3 in LSK cells of *Nol3*^{+/+} and *Nol3*^{-/-} MPN mice, under unstimulated, TPO-stimulated (50 ng/ml), and G-CSF-stimulated (10 ng/ml) conditions (*n* = 4). (F and G) Quantification of phospho-flow analysis of pSTAT5 and pSTAT3, respectively, in LSK cells from *Nol3*^{+/+} and *Nol3*^{-/-} MPN mice (MFI, mean fluorescence intensity; *n* = 4). (H) Western blot analysis of total spleen cells from *Nol3*^{+/+} and *Nol3*^{-/-} MPN mice, under unstimulated, TPO-stimulated (50 ng/ml), G-CSF-stimulated (10 ng/ml) conditions (TPO, *n* = 3; G-CSF, *n* = 2). Bars represent mean values. Error bars represent \pm SD; *, *P* < 0.05; **, *P* < 0.01; ***, *P* < 0.001.

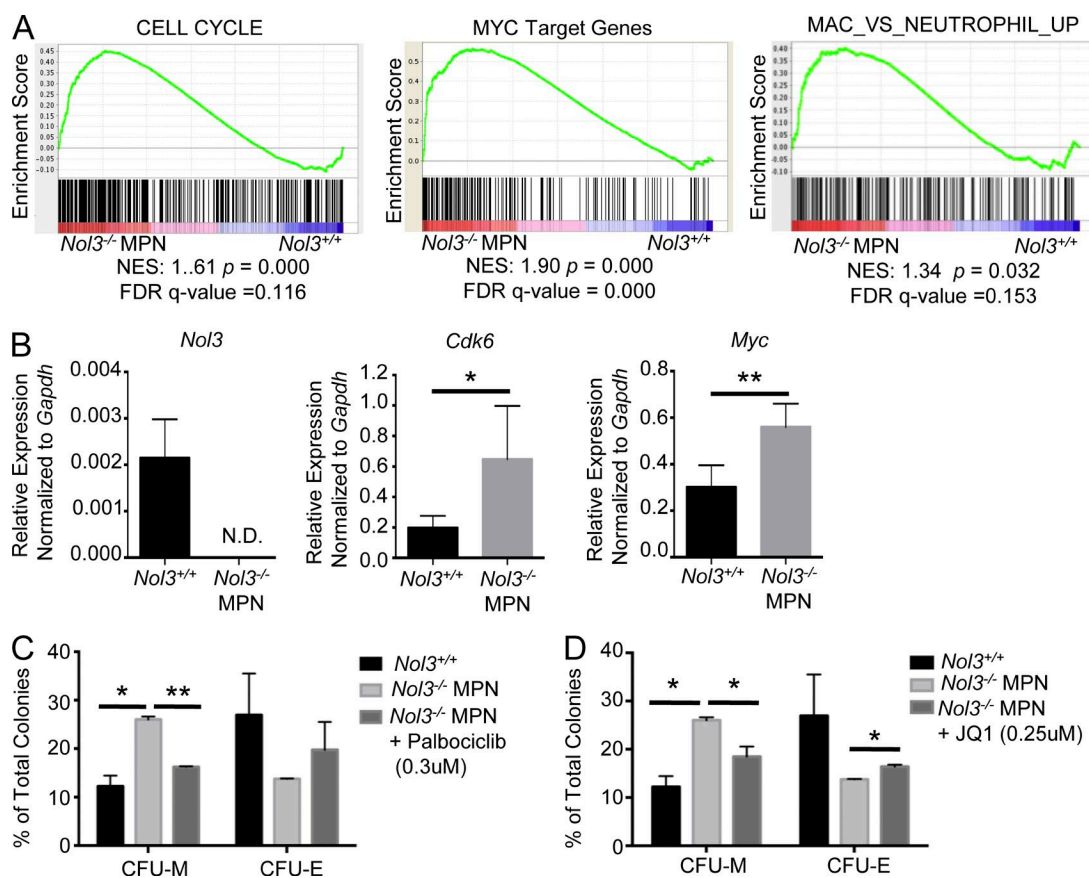


Figure 7. ***Cdk6* and *Myc* are functionally relevant downstream targets in *Nolz*^{-/-} MPN.** (A) GSEA of pathways enriched in *Nolz*^{-/-} MPN Thy1⁺LSK cells compared with *Nolz*^{+/+} Thy1⁺LSK cells. (B) Validation of *Nolz* and dysregulated genes of interest from individual *Nolz*^{+/+} ($n = 6$) and individual *Nolz*^{-/-} MPN Thy1⁺LSK ($n = 4$) cells by qPCR. (C) Colony formation assay of sorted Thy1⁺LSK or LSK cells isolated from *Nolz*^{+/+} and *Nolz*^{-/-} MPN bone marrow or spleen and treated with DMSO or the CDK4/6 inhibitor Palbociclib Isethionate ($n = 2$). (D) Colony formation assay of sorted Thy1⁺LSK or LSK cells isolated from *Nolz*^{+/+} and *Nolz*^{-/-} MPN bone marrow or spleen and treated with DMSO or JQ1 ($n = 2$). Bars represent mean values. Error bars represent \pm SD; *, $P < 0.05$; **, $P < 0.01$.

to stimulation by either TPO or G-CSF; cytokines elevated and implicated in MPN (Panteli et al., 2005). Activation of both STAT5 and STAT3 is present in *Nolz*^{-/-} MPN mice and subsequently leads to elevation of downstream effectors *Cdk6* and *Myc* (Fukada et al., 1998; Kiuchi et al., 1999; Lin et al., 2012; Pinz et al., 2016), which we found to be functionally relevant targets in *Nolz*^{-/-} MPN stem cells.

ARC has primarily been described in the context of apoptosis inhibition of the extrinsic and intrinsic apoptosis pathways in many tissues. Our study has uncovered a novel tumor suppressor-like function for ARC within the hematopoietic system. In support of new functions of ARC, several recent papers have shown that ARC can negatively regulate NF- κ B signaling and that it may also serve a tumor suppressor role in renal cell carcinoma cells (Kung et al., 2014; Gobe et al., 2016). Our study further suggests dual roles for *Nolz*/ARC in oncogenesis and hematopoiesis that may be cell context- and cell type-dependent. ARC has been reported to localize to both the cytoplasm and the nucleus, depending on

cell type. ARC is primarily cytoplasmic in most cell types that have been studied; however, it has been reported to localize to the nucleus in some solid tumor cell lines in one study (Mercier et al., 2005; Wang et al., 2005). Interestingly, Western blot fractionation experiments of four AML cell lines show that ARC protein expression is primarily localized to the cytoplasm (Fig. S1 N), supporting a cytoplasmic function for ARC in normal and malignant hematopoiesis.

Given that loss of *Nolz*/ARC leads to increased JAK-STAT activation in mouse hematopoiesis, and that ectopic expression of ARC in MPN cell lines leads to repression of JAK-STAT signaling, our data provide evidence for ARC as a negative modulator of JAK-STAT signaling in the context of the hematopoietic system. ARC could, for instance, be behaving as a scaffolding protein downstream of hematopoietic cytokine receptors that has the ability to inhibit signaling, similar to other scaffolding proteins involved in MPN, such as LNK (Tong and Lodish, 2004; Oh et al., 2010). Further studies are warranted to investigate these interesting possibilities.

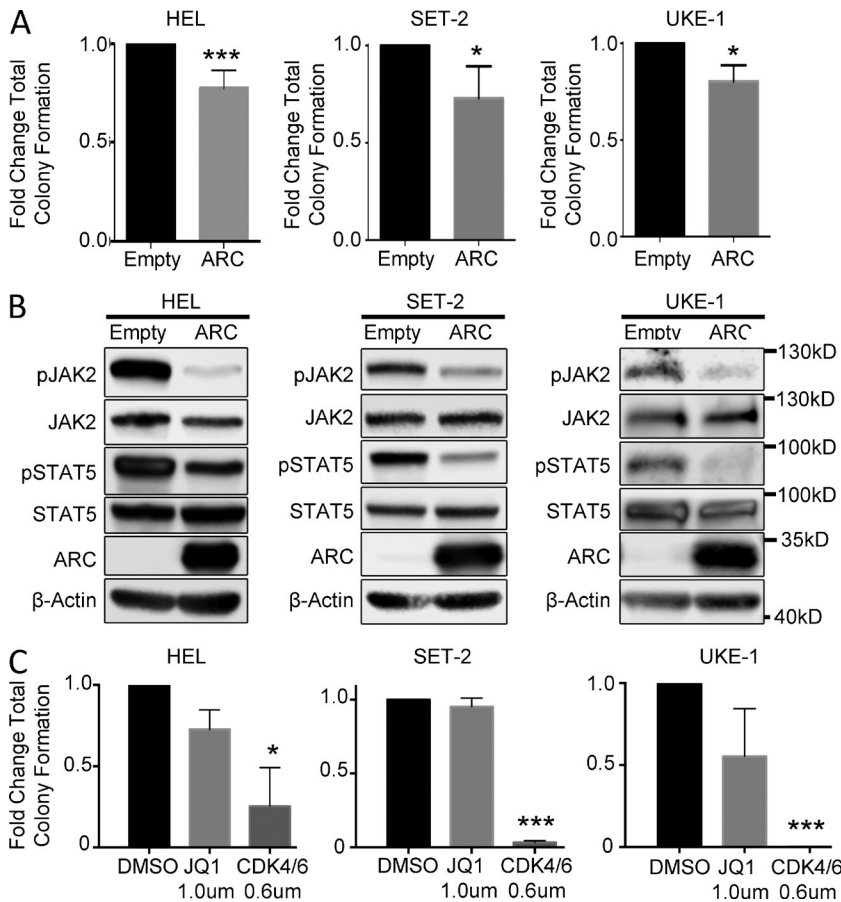


Figure 8. Ectopic expression of ARC in human MPN cell lines leads to decreased colony formation and negative regulation of JAK-STAT signaling. (A) Colony formation assays of HEL ($n = 5$), SET-2 ($n = 3$), and UKE-1 ($n = 3$) cells transduced with either empty vector control or human ARC-expressing lentivirus. (B) Western blot analysis of HEL, SET-2, and UKE-1 cells transduced with either empty or human ARC-expressing vector ($n = 3$). (C) Colony formation assay of HEL, SET-2, and UKE-1 cells treated with DMSO, JQ1, or the CDK4/6 inhibitor Palbociclib Isethionate ($n = 2$). Bars represent mean values. Error bars represent \pm SD; *, $P < 0.05$; ***, $P < 0.001$.

Gene expression analysis showed that *NOL3* is decreased in $CD34^+$ cells in the majority of PMF patients, and SNP array data showed *NOL3* deletion occurs, albeit not at a high frequency, in patients with myeloid malignancies. Importantly, 0/72 healthy controls assayed by SNP array had UPD/deletion of *NOL3*, suggesting that *NOL3* loss specifically occurs in patients with myeloid malignancies. Mutational data were available in four of the 17 patients with *NOL3* deletion (Table S2), and additional investigation of TCGA AML patient data showed five patients with either deep or shallow deletions of *NOL3*. 3/9 *NOL3* deletion patients from these two datasets in which mutational data were available showed mutations in *TP53*. All other leukemia-related mutations did not occur more than once. Interestingly, *JAK2V617F* and *TP53* mutations coexist in the SET-2 cell line, as well as the HEL cell line, which additionally harbors a deletion containing the *NOL3* locus (Zhao et al., 2012). The association of *NOL3* deletion and *TP53* mutational status may be relevant, as ARC has been shown to bind and inhibit p53 function in the context of malignancy (Foo et al., 2007). Interestingly, there was no obvious correlation with *NOL3* expression and deletion; however, the samples used in the SNP array were unfractionated bulk cells, and our data suggest that *NOL3* is primarily expressed at the stem and progenitor cell level; further studies using precisely fractionated immature cell types will be required.

In summary, our studies provide a novel mouse model in which genetic deletion of *Nol3* leads to development of a transplantable MPN that resembles PMF and shares key phenotypic, cell biological, and molecular characteristics with human disease. *Nol3*^{-/-}-induced disease is characterized by an expanded immature $Thy1^+LSK$ cell population that is actively proliferating and skewed toward myelomonocytic differentiation. Molecularly, this phenotype is mediated by increased activation of STAT5 and STAT3, leading to functionally relevant up-regulation of *Cdk6* and *Myc*. Furthermore, we found *NOL3* levels to be decreased in $CD34^+$ cells of the majority of patients with PMF, and identified deletions of the *NOL3* gene locus in a subset of patients with different myeloid malignancies. Our study provides a new PMF-like mouse model and reveals a novel tumor suppressor role of *NOL3* in the pathogenesis of MPN.

MATERIALS AND METHODS

Mice

Nol3^{-/-} mice (deletion encompassing the entire open reading frame of ARC) were kindly provided by R.N. Kitis (Albert Einstein College of Medicine, Bronx, NY) (Zaiman et al., 2011). *Nol3*^{+/+} and *Nol3*^{-/-} mice were age matched for all experimental studies. C57BL/6 SJL-*Ptprca*^a *Pepc*^b/BoyJ

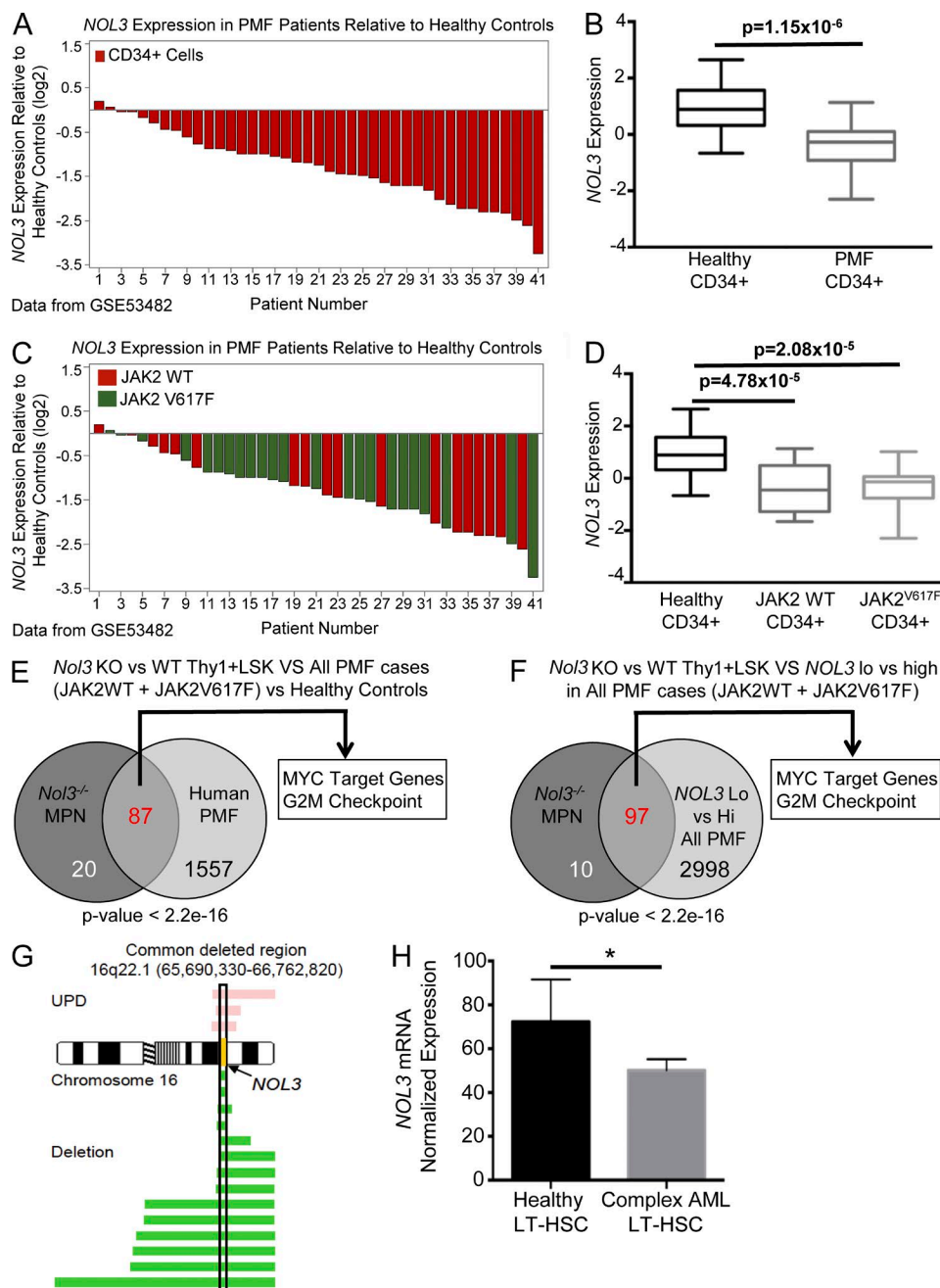


Figure 9. *Nol3*-deficient Thy1⁺LSK cells have a molecular phenotype similar to human PMF, and *NOL3* is deleted and down-regulated in patients with myeloid malignancies. (A) Waterfall plot of *NOL3* expression in CD34⁺ cells from 41 patients with PMF relative to the mean expression of *NOL3* in CD34⁺ cells from 16 healthy controls (GEO accession no. GSE53482). (B) Box plot summary of *NOL3* expression in CD34⁺ cells from patients with PMF in comparison to CD34⁺ cells from healthy controls (GSE53482). (C) Waterfall plot of relative expression of *NOL3* in CD34⁺ cells from 41 patients with PMF (same data as in A) with indicated JAK2V617F mutation status relative to the mean expression of *NOL3* in CD34⁺ cells from 16 healthy controls (GSE53482). (D) Box plot summary of *NOL3* expression in CD34⁺ cells from patients with PMF with or without JAK2V617F mutations in comparison to CD34⁺ cells from healthy donors (GSE53482). (E) Comparative GSEA analysis depicting significantly positively enriched gene sets (FDR q-value < 0.01) in *Nol3*^{-/-} MPN (vs. *Nol3*^{+/+}) Thy1⁺LSK cells and CD34⁺ cells from PMF patients (vs. healthy controls). $P < 2.2 \times 10^{-16}$; odds ratio, 28.19. (F) Comparative GSEA analysis depicting significantly positively enriched gene sets (FDR q-value < 0.01) in *Nol3*^{-/-} MPN (vs. *Nol3*^{+/+}) Thy1⁺LSK cells and CD34⁺ cells from PMF patients dichotomized by high and low *NOL3* expression. $P < 2.2 \times 10^{-16}$; odds ratio, 27.99. (G) Commonly deleted region (hg18) on chromosome 16 in human patients with myeloid malignancies. Yellow, *NOL3* locus; pink bars, length of region with UPD; green bars, length of chromosomal deletion. (H) *NOL3* mRNA normalized expression in sorted LT-HSCs from healthy control subjects ($n = 4$) and from patients with complex karyotype AML ($n = 5$). Bars represent mean values. Error bars represent \pm SD; *, $P < 0.05$.

wild-type CD45.1⁺ mice were purchased from The Jackson Laboratory. All mice were housed in a special pathogen-free (SPF) barrier facility. All animal experiments were performed in compliance with institutional guidelines and approved by the Animal Institute Committee of the Albert Einstein College of Medicine (#20130102).

Cell counts

Total bone marrow cell counts were determined from tibiae, pelvic bones, and femurs for each mouse after erythrocyte lysis using ACK buffer, pH 7.4 (0.15 M NH₄Cl, 10 mM KHCO₃, and 1.0 mM EDTA). Spleen cell counts were determined from entire spleen tissue after erythrocyte lysis.

Complete blood counts

Peripheral blood was obtained from the facial vein of living mice or heart of euthanized mice and analyzed using the Forcyte Hematology Analyzer (Oxford Science Inc.) according to the manufacturer's instructions.

Cell lines

The AML cell lines HEL 92.1.7, HL-60, MV4-11, and THP-1 were purchased from the American Type Culture Collection and grown in IMDM or RPMI medium supplemented with 10% FBS and 1% penicillin/streptomycin. The MOLM-14 cell line was obtained from the German Collection of Microorganisms and Cell Cultures (DSMZ) and grown in RPMI supplemented with 10% FBS and 1% penicillin/streptomycin. The SET-2 and UKE-1 cell lines were gifts from R. Levine (Memorial Sloan-Kettering Cancer Center, New York, NY). SET-2 cells were grown in RPMI medium supplemented with 10% FBS and 1% penicillin/streptomycin. UKE-1 cells were grown in IMDM supplemented with 10% FBS, 10% Horse Serum, 1 μ M hydrocortisone, and 1% penicillin/streptomycin.

Lentiviral vectors and transduction

For reexpression studies, we introduced a DNA coding sequence that codes for human ARC protein into the EcoRI site of a pCAD-IRES-GFP lentiviral construct (Steidl et al., 2007). For production of lentiviral particles, lentiviral expression constructs were transfected together with packaging vectors into 293T producer cells using Eugene HD transfection reagent (Roche), supernatants were harvested after 48 and 72 h. The HEL, SET-2, and UKE-1 cell lines were transduced with human ARC coding IRES-GFP containing lentivirus (MOI 10). For expression of ARC in cell lines, spinfection of the lentiviral supernatant, incubated with 10 μ g/ml polybrene for 1 h at 37°C and 1,000 RCF was performed. Cells were then put in culture and media was added 3 h after spinfection. After 48 h in culture at 37°C, the cells were washed with PBS and transduction efficiency was determined by flow cytometry. GFP⁺ cells were sorted using a FACS Aria II sorter (BD) and used for experiments.

Histology

Femurs, spleens, and livers were fixed for >24 h in 10% neutral buffered formalin at room temperature and subject to paraffin embedding according to standard protocols. Sections were cut using a microtome and were stained for H&E for histological analysis, reticulin stain for detection of reticulin fibers, and myeloperoxidase for detection of active myelopoiesis. Sections were imaged using EVOS Cell Imaging Station (Life Technologies) with 4 \times , 10 \times , 20 \times , and 50 \times objective lenses.

Western blotting

Lysates from whole heart tissue, whole bone marrow (after erythrocyte lysis), FACS-purified Lin⁺, Lin⁻c-kit⁺ bone marrow cells, and cell lines were prepared using modified RIPA buffer with protease and phosphatase inhibitors. Cells were lysed for 10 min at 4°C and sonicated at 4°C for 10 min. 8 μ g of heart protein lysates, 150 μ g of total bone marrow protein lysates, and 125 μ g of sorted cell protein lysates were resolved on 10% polyacrylamide gels for SDS-PAGE. For fractionation, cells were first lysed with a modified cytoplasmic RIPA buffer, and then cytoplasmic fractions were isolated. Remaining nuclear pellets were lysed with a complete RIPA buffer and then sonicated for 10 min. For phospho-Western analysis, HEL, SET-2, and UKE-1 cells were lysed in a modified RIPA buffer with protease and phosphatase inhibitors, and 50 μ g of lysate was used. From total spleen, 2 \times 10⁶ cells were stimulated with 50 ng/ml TPO, 10 ng/ml G-CSF, or PBS (unstimulated), and then lysed in modified RIPA buffer with protease and phosphatase inhibitors and subsequently resolved on 10% polyacrylamide gels. Immunoblotting was performed with a rabbit polyclonal antibody against ARC (1:200; Cayman Chemical) or Lamin-B1 (1:1,000; Abcam), and a monoclonal rabbit antibody against β -actin (1:1,000; Sigma-Aldrich). For phospho-western, membranes were incubated with polyclonal rabbit antibodies against JAK2 (1:1,000; Cell Signaling Technology), phospho-JAK2 (Tyr1007/1008; 1:1,000; Cell Signaling Technology), STAT5 (1:1,000; Cell Signaling Technology), phospho-STAT5 (Tyr694; 1:1,000; Cell Signaling Technology), STAT3 (1:1,000; Cell Signaling Technology), and phospho-STAT3 (Tyr705; 1:1,000; Millipore). Primary antibodies were incubated overnight at 4°C in blocking solution (PBS containing 0.1% [vol/vol] Tween-20 with 5% [wt/vol] nonfat dry milk powder) or 2% BSA in PBS. Secondary antibody anti-rabbit IgG horseradish peroxidase (HRP)-conjugated (Santa Cruz Biotechnology, Inc.) at either 1:5,000 or 1:10,000 dilution was used for detection of primary antibodies. Membranes were washed in blocking solution or PBS 0.1% Tween-20 (last wash) and primary antibody signal was detected using the Pierce ECL Western Blotting Substrate or SuperSignal West Femto Maximum Sensitivity Substrate kit (Thermo Fisher Scientific).

Flow cytometry

All antibodies used were purchased from eBioscience unless otherwise stated. Total bone marrow cells were isolated from tibiae, femurs, and pelvic bones by gentle crushing in PBS, followed by erythrocyte lysis with ACK buffer.

For analysis of mature spleen, bone marrow and peripheral blood cell populations: Cells were stained with antibodies Gr-1 (RB6-8C5), CD11b (M1/70), TER-119 (TER-119), CD71 (R17217), CD41 (eVioMWR30), CD8A (53-6.7), CD4 (GK1.5), and B220 (RA3-6B2).

For analysis of hematopoietic stem and progenitor cells: bone marrow or spleen cells were stained with a cocktail for lineage markers CD3e (145-2C11), CD4 (GK1.5), CD8a (53-6.7), CD19 (eBio1D3), Ter119 (TER-119), B220 (RA3-6B2), Gr-1 (RB6-8C5), CD11b (M1/70), and lineage-negative cells were analyzed for cKit (2B8), SCA-1 (D7; BioLegend), CD34 (RAM34), CD16/CD32 (93), FLT-3/FLK2 (A2F10), and Thy-1.2 (53-2.1) expression and streptavidin. Cells were sorted and analyzed using either a FACS Aria or 5-laser FACS Aria II Special Order System flow cytometer (BD). Analysis of FACS data were performed using FACSDiva (BD) and FlowJo (Tree Star) software.

Phospho-flow cytometry

Protocol adapted from (Kalaitzidis and Neel, 2008). In brief, lineage-depleted bone marrow cells from 10–14-mo-old wild-type and *Nol3*^{-/-} MPN mice were incubated in IMDM 2% FBS for 30 min before cytokine stimulation. Cells were then stimulated with 50 ng/ml TPO, 10 ng/ml G-CSF, or PBS (unstimulated) for 15 min. After stimulation, cells were fixed using equal volume of Phosflow Fix Buffer I (BD) for 10 min at 37°C. Cells were pelleted by centrifugation for 5 min at 300 g, and after removal of supernatant, permeabilized using ice-cold acetone dropwise and incubated for 10 min on ice. Cells were then washed twice with 2% FBS in PBS, and stored in 2% FBS in PBS at 4°C until flow cytometry analysis. Samples were analyzed at the same time using a BD LSR II flow cytometer and antibodies against phospho-STAT5 (BD) and phospho-STAT3 (BD).

Ki-67 and Hoechst staining

All antibodies used were purchased from eBioscience unless otherwise stated. Total bone marrow cells were stained with a cocktail for lineage markers CD3e (145-2C11), CD4 (GK1.5), CD8a (53-6.7), CD19 (eBio1D3), Ter119 (TER-119), B220 (RA3-6B2), Gr-1 (RB6-8C5), CD11b (M1/70), and lineage-negative cells were analyzed for c-Kit (2B8), SCA-1 (D7), FLT-3 (A2F10), and Thy-1.2 (53-2.1) expression. Cells were washed with PBS 2% FBS and fixed with Cytofix/Cytoperm (BD) for 20 min at 4°C. Cells were then washed twice with PermWash buffer (BD), and resuspended in 100 µl of PermWash buffer with FITC conjugated Anti-Ki-67 antibody (BD) and incubated overnight at 4°C. Before analysis bone marrow cells were incubated with Hoechst 33342 (1:400 dilution) for 10 min on ice.

Annexin V staining

Bone marrow and spleen cells were isolated as previously described. Staining was performed according to the manufacturer's instructions with the Annexin-V FLUOS Staining kit (Roche). 49,6-diamidino-2-phenylindole (DAPI; 1:1,000) was used to identify live cells. Viable cells were defined as Annexin-V⁻/DAPI⁻.

Transplantation experiments

Total bone marrow or spleen single-cell suspensions were harvested and erythrocytes were lysed using ACK buffer. Live cells were counted via Trypan blue exclusion and were resuspended in HBSS (Thermo Fisher Scientific). For all transplantation experiments unless otherwise specified, recipient mice were lethally irradiated (950–1,050 rads) using a Shepherd 6810 ¹³⁷Cs irradiator and received retroorbital injections for cell transplantation 4 h after irradiation. For all transplantation experiments engraftment of donor cells was monitored by FACS analysis of peripheral blood after transplantation using CD45.1 (A20) and CD45.2 (104) antibodies.

Transplantation of *Nol3*^{-/-} MPN. Lethally irradiated SJL-*Ptprc*^a *Pepc*^b/BoyJ wild-type CD45.1⁺ recipient mice were injected with *Nol3*^{+/+} or *Nol3*^{-/-} MPN CD45.2⁺ 1–5 × 10⁶ bone marrow cells or 6–10 × 10⁶ spleen cells. For each individual *Nol3*^{+/+} or *Nol3*^{-/-} MPN donor mouse 1–5 recipient mice were transplanted. All mice evaluated for MPN disease initiation in recipient mice had (89–99%) donor peripheral blood engraftment. Mice were sacrificed 6–8 mo after transplantation for bone marrow transplantations or 5–7 mo after transplantation for spleen transplantations for detection of donor-derived disease.

Competitive transplantation experiments. Lethally irradiated wild-type SJL-*Ptprc*^a *Pepc*^b/BoyJ CD45.1⁺ recipient mice were co-injected intravenously with a mixture of 1–2 × 10⁶ wild-type CD45.1⁺ or wild-type CD45.1/CD45.2⁺ whole bone marrow competitor cells and 1–2 × 10⁶ of either *Nol3*^{+/+} or *Nol3*^{-/-} MPN CD45.2⁺ whole bone marrow cells in a 1:1 ratio. Each individual recipient mouse was the recipient of bone marrow cells from one individual *Nol3*^{+/+} or *Nol3*^{-/-} MPN mouse for each experiment, in addition to the competitor bone marrow, which was aliquoted from a pool that was common for the whole experiment. The experiment was performed twice with two independent *Nol3*^{+/+} or *Nol3*^{-/-} MPN bone marrows. For LT-HSC competitive transplantation, 1,325 sorted Thy1⁺LSK cells from CD45.1⁺ wild-type mouse bone marrow was mixed in a 1:1 ratio with 1,325 sorted Thy1⁺LSK cells from CD45.2⁺ *Nol3*^{+/+} or *Nol3*^{-/-} MPN bone marrow and transplanted via direct femoral injection into lethally irradiated SJL-*Ptprc*^a *Pepc*^b/BoyJ CD45.1⁺ recipient mice, along with 100,000 CD45.1 supporting cells. Peripheral blood engraftment was analyzed every 4 wk for 16 wk.

Reciprocal transplantation experiments. Lethally irradiated 3-mo-old CD45.2⁺ *Nol3*^{+/+} or *Nol3*^{-/-} mice were injected intravenously with 3–5 × 10⁶ FACS purified wild-type CD45.1⁺ total bone marrow cells. Donor cell engraftment was detected via peripheral blood FACS analysis after transplantation. Mice were sacrificed 11–12 mo after transplantation for analysis of donor-derived MPN. 2/13 *Nol3*^{-/-} recipient mice had <35% donor cell chimerism and were excluded for evaluation of donor-derived MPN including spleen size and complete blood count.

Colony assays

For stem and progenitor cell colony assays, cells were FACS purified and 400–1,200 cells/ml were plated in HSC007 methylcellulose (R&D Systems). Cytospins of single-cell suspensions from colony assays were stained using a modified Giemsa stain (Shandon Kwik-Diff Stains; Thermo Fisher Scientific) according to the manufacturer's protocol. Cell morphology was evaluated using an EVOS FL Auto microscope (Life Technologies). For peripheral blood colony assays, 30 µl of peripheral blood freshly isolated from the heart of euthanized mice was added to 270 µl of IMDM 2% FBS and resuspended in HSC007 methylcellulose. For HEL, SET-2, and UKE-1 cell line colony assays, sorted GFP⁺ cells were plated in HSC002SF methylcellulose (R&D Systems). All scored colonies had >40 cells/colony. All colonies were scored after 7–10 d of culture at 37°C, 5% CO₂.

Inhibitor treatment

FACS-sorted *Nol3*^{+/+} and *Nol3*^{-/-} MPN Thy1⁺LSK or LSK cells isolated from bone marrow or spleen were plated in HSC007 in the presence of either DMSO, 300 nM CDK4/CDK6 inhibitor Palbociclib Isethionate (Sigma-Aldrich), or 250 nM Myc inhibitor JQ1 (Sigma-Aldrich). Inhibitors were prepared in DMSO and plated in a total volume of 2 µl/ml. For HEL, SET-2, and UKE-1 cell lines, cells were plated in HSC002SF in the presence of either DMSO, 1 µM JQ1, or 600 nM Palbociclib. All colonies were scored after 7–10 d of culture at 37°C, 5% CO₂.

Isolation of serum and serum cytokine array

Serum was isolated from peripheral blood harvested from the heart of euthanized mice and was spun down at 450 g for 10 min. The supernatant was transferred and the spin was repeated. The supernatant was then stored at –80°C until use. 6 *Nol3*^{+/+} and 6 *Nol3*^{-/-} MPN serum samples were pooled separately and diluted 1:10 and used as lysate according to the manufacturer's instructions for Mouse Angiogenesis Antibody Array (Affymetrix, MA6320). Immunoblots were quantified using ImageJ software (National Institutes of Health).

Real-time PCR

RNA for real-time quantitative PCR was extracted from isolated cell populations using the RNeasy Micro kit (QIAGEN) and RNA was reverse transcribed to cDNA using Superscript

II (Invitrogen). For some samples RNA was extracted using Dynabeads mRNA DIRECT kit (Ambion) and converted to cDNA using RNA to cDNA EcoDRY Premix (Random Hexamers; Takara Bio Inc.). Amplification of target genes was measured using the Universal PCR Power SYBR Green mix (Applied Biosystems). cDNA was amplified in a final volume of 15 µl in 96-well or 384-well microtiter plates according to the manufacturer's recommendation. Primers used for real-time PCR are as follows: *Nol3* forward, 5'-AGTTCGAAGAAATGGGCAAC-3'; reverse, 5'-GCATCCAAGGCTTCGTACTC-3'; *c-Myc* forward, 5'-ACAGGACTCCCCAGGCTCCG-3'; reverse, 5'-CGTGGCTGTCTGCGGGGTTT-3'; *Cdk6* forward, 5'-CCTTACCTCGGTGGTCGTC-3'; reverse, 5'-GAACCTCCACGAAAAAGAGGCT-3'; *Gapdh* forward, 5'-CCAGCCTCGTCCCGTAGAC-3'; reverse, 5'-GCCTTGACTGTGCCGTTGA-3'. All real-time PCR experiments were performed using a ViiA7 instrument (Life Technologies) with one cycle of 50°C (2 min) and 95°C (10 min), followed by 40 cycles of amplification, with each cycle comprising the steps: 95°C (15 s) and 60°C (for 1 min). Specific amplification of the target gene products was validated by melting curve analysis and Sanger sequencing. Target gene expression quantification was calculated using the Pfaffl model and normalized to *Gapdh* expression levels.

Analysis of microarray data

RNA for microarray was extracted from FACS purified Thy1⁺LSK cells using the RNeasy Micro kit (QIAGEN). RNA quantity and quality was assessed using a 2100 Bioanalyzer (Agilent). For global gene expression analysis, isolated RNA was amplified using the WT Ovation Pico RNA amplification system (Nugen). After labeling with the GeneChip WT terminal labeling kit (Affymetrix), labeled cRNA of each individual sample was hybridized to an Affymetrix Mouse Gene 2.0ST microarray (Affymetrix), stained and scanned by GeneChip Scanner 3000 7 G system (Affymetrix) according to standard protocols. Raw data were normalized using Expression Console Software (Affymetrix) and analyzed using Transcriptome Analysis Console Software (Affymetrix). Unannotated and sex-specific genes varying among samples were removed for analysis. Gene set enrichment analysis was performed using the gene set enrichment analysis tool (GSEA; Broad Institute).

GEO

Gene expression data generated from Thy1⁺LSK cells isolated from *Nol3*^{+/+} and *Nol3*^{-/-} MPN mice are provided under accession no. GSE76121.

Datasets

For human PMF gene expression comparative analysis, we used the publicly available GEO dataset under accession no. GSE53482 (healthy controls, *n* = 16; PMF patients, *n* = 41) consisting of gene expression data of fractionated CD34⁺ cells isolated from peripheral blood of healthy controls and pa-

tients with PMF. Box plots of *NOL3* expression data were generated using QluCore Omics Explorer software (QluCore). Waterfall plots for *NOL3* expression in PMF patients were created using the SAS statistical analysis software (SAS Institute Inc.). *NOL3* expression data in AML and healthy control LT-HSCs were analyzed using previously reported, publically available datasets (Barreyro et al., 2012; Schinke et al., 2015).

Comparative analysis with published datasets

For GSEA comparative analysis, we compared GSEA results of differentially expressed genes between murine *Nol3*^{-/-} MPN Thy1⁺LSK cells (versus age-matched *Nol3*^{+/+}) and human PMF CD34⁺ cells (GEO accession no. GSE53482) versus healthy controls. Data from PMF patients were then dichotomized into *NOL3* high and low expression groups based on a threshold of *NOL3* expression of 3.85. Significant positive enrichment was identified using FDR *q*-values < 0.01.

Statistics

For PMF and AML analyses, Fisher's exact test of independence was used to assess correlations of overlapping GSEA pathways in human PMF and *NOL3* expression in human de novo AML. Throughout this study, P values are by 2-tailed Student's *t* test and error bars represent the mean ± SD unless otherwise indicated. Statistical analysis of group comparisons was performed using Student's *t* test in Excel or GraphPad Prism. A value of *P* < 0.05 was used to determine whether a significant difference existed between two groups.

Online supplemental material

Fig. S1 shows ARC expression in different hematopoietic cell types, additional analyses of hematopoietic organs pre- and post-transplantation, and subcellular localization of ARC protein. Table S1 lists peripheral blood counts. Table S2 lists Characteristics of patients with myeloid malignancies with *NOL3* deletion or UPD (hg18).

ACKNOWLEDGMENTS

We thank J. Filipa Leite and J. Chan for their guidance and technical expertise. We also thank D. Sun and G. Simkin of the Stem Cell Isolation and Xenotransplantation Core Facility (funded by NYSTEM grant #C029154) of the Gottesman Institute for Stem Cell and Regenerative Medicine Research for expert technical support, W. Tran from the Einstein Genomics Core Facility, and P. Schultes from the Einstein Department of Cell Biology for technical assistance.

This work was supported by National Institutes of Health (NIH) grants to U. Steidl (R01CA166429) and K. Gritsman (R01CA196973), an MSTP training grant to R.F. Stanley and R.T. Piszczatowski. (T32GM007288), National Heart, Lung, and Blood Institute Fellowship to R.F. Stanley (F30HL122085), the NIH Cellular and Molecular Biology and Genetics Training Grant to R.F. Stanley, K. Mitchell, and W.M. McKimpson (T32GM007491). R.N. Kitsis was supported by the Dr. Gerald and Myra Dorros Chair in Cardiovascular Disease. U. Steidl is the Diane and Arthur B. Belfer Scholar in Cancer Research of the Albert Einstein College of Medicine, and is a Research Scholar of the Leukemia & Lymphoma Society.

The authors declare no competing financial interests.

Author contributions: R.F. Stanley designed and performed research, conducted experiments, analyzed data, made figures, and wrote the manuscript; R.T. Piszczatowski designed and performed research, conducted experiments, analyzed data,

made figures, and wrote the manuscript; B. Bartholdy designed research, interpreted data, and performed statistical analyses; K. Mitchell conducted experiments and interpreted data; W.M. McKimpson provided reagents and interpreted data; S. Narayanagari conducted experiments; D. Walter conducted experiments and interpreted data; T.I. Todorova conducted experiments; C. Hirsch analyzed and interpreted data; C. McMahon interpreted data; K. Gritsman designed experiments and interpreted data; B. Will and R.N. Kitsis designed research and analyzed and interpreted data; H. Makishima, C. Hirsch, and J.P. Maciejewski provided clinical data; U. Steidl designed research, analyzed data, and contributed to writing of the manuscript.

Submitted: 11 December 2016

Revised: 4 January 2017

Accepted: 5 January 2017

REFERENCES

- Abdel-Wahab, O., A. Pardanani, O.A. Bernard, G. Finazzi, J.D. Crispino, H. Gisslinger, R. Kralovics, O. Odenike, K. Bhalla, V. Gupta, et al. 2012. Unraveling the genetic underpinnings of myeloproliferative neoplasms and understanding their effect on disease course and response to therapy: proceedings from the 6th International Post-ASH Symposium. *Am. J. Hematol.* 87:562–568. <http://dx.doi.org/10.1002/ajh.23169>
- Adamson, J.W., P.J. Fialkow, S. Murphy, J.F. Prchal, and L. Steinmann. 1976. Polycythemia vera: stem-cell and probable clonal origin of the disease. *N. Engl. J. Med.* 295:913–916. <http://dx.doi.org/10.1056/NEJM197610212951702>
- Andréasson, B., B. Swolin, and J. Kutti. 2002. Patients with idiopathic myelofibrosis show increased CD34⁺ cell concentrations in peripheral blood compared to patients with polycythaemia vera and essential thrombocythaemia. *Eur. J. Haematol.* 68:189–193. <http://dx.doi.org/10.1034/j.1600-0609.2002.01610.x>
- Barreyro, L., B. Will, B. Bartholdy, L. Zhou, T.I. Todorova, R.F. Stanley, S. Ben-Neriah, C. Montagna, S. Parekh, A. Pellagatti, et al. 2012. Overexpression of IL-1 receptor accessory protein in stem and progenitor cells and outcome correlation in AML and MDS. *Blood*. 120:1290–1298. <http://dx.doi.org/10.1182/blood-2012-01-404699>
- Baxter, E.J., L.M. Scott, P.J. Campbell, C. East, N. Fourouclas, S. Swanton, G.S. Vassiliou, A.J. Bench, E.M. Boyd, N. Curtin, et al. Cancer Genome Project. 2005. Acquired mutation of the tyrosine kinase JAK2 in human myeloproliferative disorders. *Lancet*. 365:1054–1061. [http://dx.doi.org/10.1016/S0140-6736\(05\)74230-6](http://dx.doi.org/10.1016/S0140-6736(05)74230-6)
- Carter, B.Z., Y.H. Qiu, N. Zhang, K.R. Coombes, D.H. Mak, D.A. Thomas, F. Ravandi, H.M. Kantarjian, E. Koller, M. Andreeff, and S.M. Kornblau. 2011. Expression of ARC (apoptosis repressor with caspase recruitment domain), an antiapoptotic protein, is strongly prognostic in AML. *Blood*. 117:780–787. <http://dx.doi.org/10.1182/blood-2010-04-280503>
- Delmore, J.E., G.C. Issa, M.E. Lemieux, P.B. Rahl, J. Shi, H.M. Jacobs, E. Kastrits, T. Gilpatrick, R.M. Paranal, J. Qi, et al. 2011. BET bromodomain inhibition as a therapeutic strategy to target c-Myc. *Cell*. 146:904–917. <http://dx.doi.org/10.1016/j.cell.2011.08.017>
- Elf, S., N.S. Abdelfattah, E. Chen, J. Perales-Patón, E.A. Rosen, A. Ko, F. Peisker, N. Florescu, S. Giannini, O. Wolach, et al. 2016. Mutant calreticulin requires both its mutant C-terminus and the thrombopoietin receptor for oncogenic transformation. *Cancer Discov.* 6:368–381. <http://dx.doi.org/10.1158/2159-8290.CD-15-1434>
- Fialkow, P.J., G.B. Faguet, R.J. Jacobson, K. Vaidya, and S. Murphy. 1981. Evidence that essential thrombocythemia is a clonal disorder with origin in a multipotent stem cell. *Blood*. 58:916–919.
- Foo, R.S.-Y., Y.-J. Nam, M.J. Ostreicher, M.D. Metz, R.S. Whelan, C.-F. Peng, A.W. Ashton, W. Fu, K. Mani, S.-F. Chin, et al. 2007. Regulation of p53 tetramerization and nuclear export by ARC. *Proc. Natl. Acad. Sci. USA*. 104:20826–20831. <http://dx.doi.org/10.1073/pnas.0710017104>

- Fry, D.W., P.J. Harvey, P.R. Keller, W.L. Elliott, M. Meade, E. Trachet, M. Albassam, X. Zheng, W.R. Leopold, N.K. Pryer, and P.L. Toogood. 2004. Specific inhibition of cyclin-dependent kinase 4/6 by PD 0332991 and associated antitumor activity in human tumor xenografts. *Mol. Cancer Ther.* 3:1427–1438.
- Fukada, T., T. Ohtani, Y. Yoshida, T. Shirogane, K. Nishida, K. Nakajima, M. Hibi, and T. Hirano. 1998. STAT3 orchestrates contradictory signals in cytokine-induced G1 to S cell-cycle transition. *EMBO J.* 17:6670–6677. <http://dx.doi.org/10.1093/emboj/17.22.6670>
- Geertman, R., A. McMahon, and E.L. Sabban. 1996. Cloning and characterization of cDNAs for novel proteins with glutamic acid-proline dipeptide tandem repeats. *Biochim. Biophys. Acta.* 1306:147–152. [http://dx.doi.org/10.1016/0167-4781\(96\)00036-X](http://dx.doi.org/10.1016/0167-4781(96)00036-X)
- Gobe, G.C., K.L. Ng, D.M. Small, D.A. Vesey, D.W. Johnson, H. Samaratunga, K. Oliver, S. Wood, J.L. Barclay, R. Rajandram, et al. 2016. Decreased apoptosis repressor with caspase recruitment domain confers resistance to sunitinib in renal cell carcinoma through alternate angiogenesis pathways. *Biochem. Biophys. Res. Commun.* 473:47–53. <http://dx.doi.org/10.1016/j.bbrc.2016.03.048>
- Jacobson, R.J., A. Salo, and P.J. Fialkow. 1978. Agnogenic myeloid metaplasia: a clonal proliferation of hematopoietic stem cells with secondary myelofibrosis. *Blood.* 51:189–194.
- James, C., V. Ugo, J.-P. Le Couédic, J. Staerk, F. Delhommeau, C. Lacout, L. Garçon, H. Raslova, R. Berger, A. Bennaceur-Griscelli, et al. 2005. A unique clonal JAK2 mutation leading to constitutive signalling causes polycythaemia vera. *Nature.* 434:1144–1148. <http://dx.doi.org/10.1038/nature03546>
- Kalaitzidis, D., and B.G. Neel. 2008. Flow-cytometric phosphoprotein analysis reveals agonist and temporal differences in responses of murine hematopoietic stem/progenitor cells. *PLoS One.* 3:e3776. <http://dx.doi.org/10.1371/journal.pone.0003776>
- Kiuchi, N., K. Nakajima, M. Ichiba, T. Fukada, M. Narimatsu, K. Mizuno, M. Hibi, and T. Hirano. 1999. STAT3 is required for the gp130-mediated full activation of the c-myc gene. *J. Exp. Med.* 189:63–73. <http://dx.doi.org/10.1084/jem.189.1.63>
- Klampff, T., H. Gisslinger, A.S. Harutyunyan, H. Nivarthi, E. Rumi, J.D. Milosevic, N.C. Them, T. Berg, B. Gisslinger, D. Pietra, et al. 2013. Somatic mutations of calreticulin in myeloproliferative neoplasms. *N. Engl. J. Med.* 369:2379–2390. <http://dx.doi.org/10.1056/NEJMoa1311347>
- Koseki, T., N. Inohara, S. Chen, and G. Núñez. 1998. ARC, an inhibitor of apoptosis expressed in skeletal muscle and heart that interacts selectively with caspases. *Proc. Natl. Acad. Sci. USA.* 95:5156–5160. <http://dx.doi.org/10.1073/pnas.95.9.5156>
- Kralovics, R., F. Passamonti, A.S. Buser, S.-S. Teo, R. Tiedt, J.R. Passweg, A. Tichelli, M. Cazzola, and R.C. Skoda. 2005. A gain-of-function mutation of JAK2 in myeloproliferative disorders. *N. Engl. J. Med.* 352:1779–1790. <http://dx.doi.org/10.1056/NEJMoa051113>
- Kralovics, R., S.-S. Teo, S. Li, A. Theodorides, A.S. Buser, A. Tichelli, and R.C. Skoda. 2006. Acquisition of the V617F mutation of JAK2 is a late genetic event in a subset of patients with myeloproliferative disorders. *Blood.* 108:1377–1380. <http://dx.doi.org/10.1182/blood-2005-11-009605>
- Kung, G., P. Dai, L. Deng, and R.N. Kitsis. 2014. A novel role for the apoptosis inhibitor ARC in suppressing TNF α -induced regulated necrosis. *Cell Death Differ.* 21:634–644. <http://dx.doi.org/10.1038/cdd.2013.195>
- Levine, R.L., M. Wadleigh, J. Cools, B.L. Ebert, G. Wernig, B.J. Huntly, T.J. Boggon, I. Wlodarska, J.J. Clark, S. Moore, et al. 2005. Activating mutation in the tyrosine kinase JAK2 in polycythemia vera, essential thrombocythemia, and myeloid metaplasia with myelofibrosis. *Cancer Cell.* 7:387–397. <http://dx.doi.org/10.1016/j.ccr.2005.03.023>
- Lin, J.-X., P. Li, D. Liu, H.T. Jin, J. He, M. Ata Ur Rasheed, Y. Rochman, L. Wang, K. Cui, C. Liu, et al. 2012. Critical Role of STAT5 transcription factor tetramerization for cytokine responses and normal immune function. *Immunity.* 36:586–599. <http://dx.doi.org/10.1016/j.immuni.2012.02.017>
- Mak, P.Y., D.H. Mak, H. Mu, Y. Shi, P. Ruvolo, V. Ruvolo, R. Jacamo, J.K. Burks, W. Wei, X. Huang, et al. 2014a. Apoptosis repressor with caspase recruitment domain is regulated by MAPK/PI3K and confers drug resistance and survival advantage to AML. *Apoptosis.* 19:698–707. <http://dx.doi.org/10.1007/s10495-013-0954-z>
- Mak, P.Y., D.H. Mak, V. Ruvolo, R. Jacamo, S.M. Kornblau, H. Kantarjian, M. Andreeff, and B.Z. Carter. 2014b. Apoptosis repressor with caspase recruitment domain modulates second mitochondrial-derived activator of caspases mimetic-induced cell death through BIRC2/MAP3K14 signalling in acute myeloid leukaemia. *Br. J. Haematol.* 167:376–384. <http://dx.doi.org/10.1111/bjh.13054>
- McKimpson, W.M., J. Weinberger, L. Czerski, M. Zheng, M.T. Crow, J.E. Pessin, S.C. Chua Jr., and R.N. Kitsis. 2013. The apoptosis inhibitor ARC alleviates the ER stress response to promote β -cell survival. *Diabetes.* 62:183–193. <http://dx.doi.org/10.2337/db12-0504>
- Medina-Ramirez, C.M., S. Goswami, T. Smirnova, D. Bamira, B. Benson, N. Ferrick, J. Segall, J.W. Pollard, and R.N. Kitsis. 2011. Apoptosis inhibitor ARC promotes breast tumorigenesis, metastasis, and chemoresistance. *Cancer Res.* 71:7705–7715. <http://dx.doi.org/10.1158/0008-5472.CAN-11-2192>
- Mercier, I., M. Vuolo, R. Madan, X. Xue, A. Levalley, A. Ashton, J. Jasmin, M. Czaja, E. Lin, R. Armstrong, et al. 2005. ARC, an apoptosis suppressor limited to terminally differentiated cells, is induced in human breast cancer and confers chemo- and radiation- resistance. *Cell Death and Differentiation.* 682–686.15861191
- Mercier, I., M. Vuolo, J.-F. Jasmin, C.M. Medina, M. Williams, J.M. Mariadason, H. Qian, X. Xue, R.G. Pestell, M.P. Lisanti, and R.N. Kitsis. 2008. ARC (apoptosis repressor with caspase recruitment domain) is a novel marker of human colon cancer. *Cell Cycle.* 7:1640–1647. <http://dx.doi.org/10.4161/cc.7.11.5979>
- Nam, Y.-J., K. Mani, A.W. Ashton, C.-F. Peng, B. Krishnamurthy, Y. Hayakawa, P. Lee, S.J. Korsmeyer, and R.N. Kitsis. 2004. Inhibition of both the extrinsic and intrinsic death pathways through nonhomotypic death-fold interactions. *Mol. Cell.* 15:901–912. <http://dx.doi.org/10.1016/j.molcel.2004.08.020>
- Nangalia, J., C.E. Massie, E.J. Baxter, F.L. Nice, G. Gundem, D.C. Wedge, E. Avezov, J. Li, K. Kollmann, D.G. Kent, et al. 2013. Somatic CALR mutations in myeloproliferative neoplasms with nonmutated JAK2. *N. Engl. J. Med.* 369:2391–2405. <http://dx.doi.org/10.1056/NEJMoa1312542>
- Norfo, R., R. Zini, V. Pennucci, E. Bianchi, S. Salati, P. Guglielmelli, C. Bogani, T. Fanelli, C. Mannarelli, V. Rosti, et al. Associazione Italiana per la Ricerca sul Cancro Gruppo Italiano Malattie Mieloproliferative Investigators. 2014. miRNA-mRNA integrative analysis in primary myelofibrosis CD34+ cells: role of miR-155/JARID2 axis in abnormal megakaryopoiesis. *Blood.* 124:e21–e32. <http://dx.doi.org/10.1182/blood-2013-12-544197>
- Oh, S.T., E.F. Simonds, C. Jones, M.B. Hale, Y. Goltsev, K.D. Gibbs Jr., J.D. Merker, J.L. Zehnder, G.P. Nolan, and J. Gotlib. 2010. Novel mutations in the inhibitory adaptor protein LNK drive JAK-STAT signaling in patients with myeloproliferative neoplasms. *Blood.* 116:988–992. <http://dx.doi.org/10.1182/blood-2010-02-270108>
- Panteli, K.E., E.C. Hatzimichael, P.K. Bouranta, A. Katsaraki, K. Seferiadis, J. Stebbing, and K.L. Bourantas. 2005. Serum interleukin (IL)-1, IL-2, sIL-2R α , IL-6 and thrombopoietin levels in patients with chronic myeloproliferative diseases. *Br. J. Haematol.* 130:709–715. <http://dx.doi.org/10.1111/j.1365-2141.2005.05674.x>
- Pikman, Y., B.H. Lee, T. Mercher, E. McDowell, B.L. Ebert, M. Gozo, A. Cuker, G. Wernig, S. Moore, I. Galinsky, et al. 2006. MPLW515L is a novel somatic activating mutation in myelofibrosis with myeloid metaplasia. *PLoS Med.* 3:e270. <http://dx.doi.org/10.1371/journal.pmed.0030270>

- Pinz, S., S. Unser, and A. Rasche. 2016. Signal transducer and activator of transcription STAT5 is recruited to c-Myc super-enhancer. *BMC Mol. Biol.* 17:10. <http://dx.doi.org/10.1186/s12867-016-0063-y>
- Schaub, F.X., R. Jäger, R. Looser, H. Hao-Shen, S. Hermouet, F. Girodon, A. Tichelli, H. Gisslinger, R. Kralovics, and R.C. Skoda. 2009. Clonal analysis of deletions on chromosome 20q and JAK2-V617F in MPD suggests that del20q acts independently and is not one of the predisposing mutations for JAK2-V617F. *Blood*. 113:2022–2027. <http://dx.doi.org/10.1182/blood-2008-07-167056>
- Schaub, F.X., R. Looser, S. Li, H. Hao-Shen, T. Lehmann, A. Tichelli, and R.C. Skoda. 2010. Clonal analysis of TET2 and JAK2 mutations suggests that TET2 can be a late event in the progression of myeloproliferative neoplasms. *Blood*. 115:2003–2007. <http://dx.doi.org/10.1182/blood-2009-09-245381>
- Schinke, C., O. Giricz, W. Li, A. Shastri, S. Gordon, L. Barreyro, T. Bhagat, S. Bhattacharyya, N. Ramachandra, M. Bartenstein, et al.. 2015. IL8-CXCR2 pathway inhibition as a therapeutic strategy against MDS and AML stem cells. *Blood*. 125:3144–3152. <http://dx.doi.org/10.1182/blood-2015-01-62163125810490>
- Steidl, U., C. Steidl, A. Ebraldiz, B. Chapuy, H.-J. Han, B. Will, F. Rosenbauer, A. Becker, K. Wagner, S. Koschmieder, et al. 2007. A distal single nucleotide polymorphism alters long-range regulation of the PU.1 gene in acute myeloid leukemia. *J. Clin. Invest.* 117:2611–2620. <http://dx.doi.org/10.1172/JCI30525>
- Tefferi, A. 2010. Novel mutations and their functional and clinical relevance in myeloproliferative neoplasms: JAK2, MPL, TET2, ASXL1, CBL, IDH and IKZF1. *Leukemia*. 24:1128–1138. <http://dx.doi.org/10.1038/leu.2010.69>
- Tefferi, A. 2012. JAK inhibitors for myeloproliferative neoplasms: clarifying facts from myths. *Blood*. 119:2721–2730. <http://dx.doi.org/10.1182/blood-2011-11-395228>
- Tefferi, A., and A. Pardanani. 2015. Myeloproliferative Neoplasms: A Contemporary Review. *JAMA Oncol.* 1:97–105. <http://dx.doi.org/10.1001/jamaoncol.2015.89>
- Tefferi, A., R. Vaidya, D. Caramazza, C. Finke, T. Lasho, and A. Pardanani. 2011. Circulating interleukin (IL)-8, IL-2R, IL-12, and IL-15 levels are independently prognostic in primary myelofibrosis: a comprehensive cytokine profiling study. *J. Clin. Oncol.* 29:1356–1363. <http://dx.doi.org/10.1200/JCO.2010.32.9490>
- Tefferi, A., P. Guglielmelli, D.R. Larson, C. Finke, E.A. Wassie, L. Pieri, N. Gangat, R. Fjerza, A.A. Belachew, T.L. Lasho, et al. 2014. Long-term survival and blast transformation in molecularly annotated essential thrombocythemia, polycythemia vera, and myelofibrosis. *Blood*. 124:2507–2513, quiz:2615. <http://dx.doi.org/10.1182/blood-2014-05-579136>
- Tibes, R., J.M. Bogenberger, K.L. Benson, and R.A. Mesa. 2012. Current outlook on molecular pathogenesis and treatment of myeloproliferative neoplasms. *Mol. Diagn. Ther.* 16:269–283. <http://dx.doi.org/10.1007/s40291-012-0006-3>
- Tong, W., and H.F. Lodish. 2004. Lnk inhibits Tpo-mpl signaling and Tpo-mediated megakaryocytopoiesis. *J. Exp. Med.* 200:569–580. <http://dx.doi.org/10.1084/jem.20040762>
- Walkley, C.R., G.H. Olsen, S. Dworkin, S.A. Fabb, J. Swann, G.A. McArthur, S.V. Westmoreland, P. Chambon, D.T. Scadden, and L.E. Purton. 2007a. A microenvironment-induced myeloproliferative syndrome caused by retinoic acid receptor γ deficiency. *Cell*. 129:1097–1110. <http://dx.doi.org/10.1016/j.cell.2007.05.014>
- Walkley, C.R., J.M. Shea, N.A. Sims, L.E. Purton, and S.H. Orkin. 2007b. Rb regulates interactions between hematopoietic stem cells and their bone marrow microenvironment. *Cell*. 129:1081–1095. <http://dx.doi.org/10.1016/j.cell.2007.03.055>
- Wang, M., S. Qanungo, M.T. Crow, M. Watanabe, and A.-L. Nieminen. 2005. Apoptosis repressor with caspase recruitment domain (ARC) is expressed in cancer cells and localizes to nuclei. *FEBS Lett.* 579:2411–2415. <http://dx.doi.org/10.1016/j.febslet.2005.03.040>
- Wang, X., A. LeBlanc, S. Gruenstein, M. Xu, J. Mascarenhas, B. Panzera, N. Wisch, C. Parker, J.D. Goldberg, J. Prchal, et al. 2009. Clonal analyses define the relationships between chromosomal abnormalities and JAK2V617F in patients with Ph-negative myeloproliferative neoplasms. *Exp. Hematol.* 37:1194–1200. <http://dx.doi.org/10.1016/j.exphem.2009.07.003>
- Zaiman, A.L., R. Damico, A. Thoms-Chesley, D.C. Files, P. Kesari, L. Johnston, M. Swaim, S. Mozammel, A.C. Myers, M. Halushka, et al. 2011. A critical role for the protein apoptosis repressor with caspase recruitment domain in hypoxia-induced pulmonary hypertension. *Circulation*. 124:2533–2542. <http://dx.doi.org/10.1161/CIRCULATIONAHA.111.034512>
- Zhao, W., Y. Du, W.T. Ho, X. Fu, and Z.J. Zhao. 2012. JAK2V617F and p53 mutations coexist in erythroleukemia and megakaryoblastic leukemic cell lines. *Exp. Hematol. Oncol.* 1:15. <http://dx.doi.org/10.1186/2162-3619-1-15>
- Zimmer, S.N., Q. Zhou, T. Zhou, Z. Cheng, S.L. Abboud-Werner, D. Horn, M. Lecocq, R. White, A.V. Krivtsov, S.A. Armstrong, et al. 2011. Crebbp haploinsufficiency in mice alters the bone marrow microenvironment, leading to loss of stem cells and excessive myelopoiesis. *Blood*. 118:69–79. <http://dx.doi.org/10.1182/blood-2010-09-307942>